[illegible] REQUIREMENTS STUDY FOR HEAD-UP DISPLAYS

FINAL REPORT

Prepared by
T. Gold
R.F. Perry

March 1972

Jointly sponsored by
OFFICE OF NAVAL RESEARCH
NAVAL AIR SYSTEMS COMMAND
U.S. ARMY ELECTRONICS COMMAND
Contract N00014-68-C-0465
NR 213-069

NOTICE

Change of Address

Organizations receiving JANAIR Reports on the initial distribution list should confirm correct address. This list is located at the end of the report. Any change in address or distribution list should be conveyed to the Office of Naval Research, Code 461, Arlington, Virginia 22217, ATTN: JANAIR Chairman.

Disposition

When this report is no longer needed, it may be transmitted to other organizations. Do not return it to the originator or the monitoring office.

Disclaimer

The findings in this report are not to be construed as an official Department of Defense or Military Department position unless so designated by other official documents.

Security Classification

DOCUMENT CONTROL DATA - R & D

(Security classification of title, body of abstract and indexing annotation must be entered when the overall report is classified)

1. ORIGINATING ACTIVITY (Corporate author)	2a. REPORT SECURITY CLASSIFICATION
Sperry Gyroscope Division Sperry Rand Corporation Great Neck, New York 11020	Unclassified 2b. GROUP

3. REPORT TITLE

VISUAL REQUIREMENTS STUDY FOR HEAD-UP DISPLAYS

4. DESCRIPTIVE NOTES (Type of report and inclusive dates)

A final report on the problem

5. AUTHOR(S) (First name, middle initial, last name)

T. Gold and R.F. Perry

6. REPORT DATE	7a. TOTAL NO. OF PAGES	7b. NO. OF REFS
March 1972	64	17

8a. CONTRACT OR GRANT NO	9a. ORIGINATOR'S REPORT NUMBER(S)
N00014-68-C-0465 b. PROJECT NO NR 213-068 c. d.	JANAIR Report 700407 9b. OTHER REPORT NO(S) (Any other numbers that may be assigned this report)

10. DISTRIBUTION STATEMENT

Approved for public release; distribution unlimited.

11. SUPPLEMENTARY NOTES	12. SPONSORING MILITARY ACTIVITY
Joint Army Navy Aircraft Instrumentation (JANAIR)	Aeronautics Programs, Code 461, Office of Naval Research, Department of the Navy, Washington, D.C. 20360

13. ABSTRACT

An experimental study was conducted to determine the binocular disparity tolerances for pilots viewing dynamic head-up display images against a moving real world background. An existing head-up display simulator, which could generate images with controlled disparities for each eye, was modified to incorporate a background of projected motion pictures taken in flight at low altitudes. Six pilots served as test subjects, three from the Army Aviation School and three from the Naval Air Test Center. The results indicate maximum disparity levels for sustained comfortable viewing of 1.0 milliradian for vertical and convergent horizontal disparities, and 2.5 milliradians for divergent horizontal disparities. These results are the same as those obtained with the display viewed against a static real world background in a preceding study involving a different group of subjects. The results for individual subjects correlate well with data obtained in optometric examinations using the Maddox Rod test.

Some ancillary studies relating to visual requirements for head-up displays were also performed. Limiting distances for the use of stereopsis by helicopter pilots for depth perception were analytically determined. Collimated head-up display images can be used by the pilots in visual comfort when they view the ground at the relatively short distances for which stereopsis is effective. A procedure for determining the field of view required for a head-up display for a helicopter was developed.

DD FORM 1 NOV 68 1473 (PAGE 1)

S/N 0101-807-6801

Security Classification

14 KEY WORDS	LINK A		LINK B		LINK C	
	ROLE	WT	ROLE	WT	ROLE	WT
Binocular vision						
Displays						
Head-up displays						
Optics						
Stereopsis						
Vision						

FOREWORD

This report presents work performed under the Joint Army Navy Aircraft Instrumentation on Research (JANAIR) Program, a research and exploratory development program directed by the United States Navy, Office of Naval Research. Special guidance is provided to the program for the Army Electronics Command, the Naval Air Systems Command, and the Office of Naval Research through an organization known as the JANAIR Working Group. The Working Group is currently composed of representatives from the following offices:

- U.S. Navy, Office of Naval Research, Aeronautics Programs, Code 461, Arlington, Virginia 22217
  —Aircraft Instrumentation and Control Program Area

- U.S. Navy, Naval Air Systems Command, Washington, D.C.
  —Avionics Division; Navigation Instrumentation and Display Branch (NAVAIR 5337)
  —Crew Systems Division; Cockpit/Cabin Requirements and Standards Branch (NAVAIR 5313)

- U.S. Army, Army Electronics Command, Avionics Laboratory, Fort Monmouth, New Jersey
  —Instrumentation Technical Area (AMSEL-VL-I)

The Joint Army Navy Aircraft Instrumentation Research Program objective is to conduct applied research using analytical and experimental investigations for identifying, defining, and validating advanced concepts which may be applied to future, improved naval and army aircraft instrumentation systems. These systems include sensing elements, data processors, displays, controls, and man/machine interfaces for fixed and rotary wing aircraft for all flight regimes.

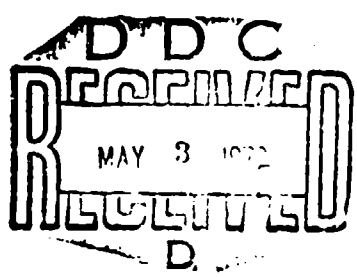

CONTENTS

LIST OF ILLUSTRATIONS

LIST OF TABLES

VISUAL REQUIREMENTS STUDY FOR HEAD-UP DISPLAYS

INTRODUCTION

The head-up display is a relatively new cockpit display technique which provides flight control information to the pilot visually as he looks through the windshield in the forward direction. The pilot has the visual impression that the images generated by optical projection are located in the real world, in front of the aircraft. These images are called virtual images because the light rays which produce them do not emanate from their apparent locations.

A research program to establish quantitative optical design tolerances for head-up displays had been conducted for the JANAIR Committee (1). The emphasis in this study was on the absolute tolerance of pilots for horizontal and vertical binocular disparities. The effects of display motion, image brightness, line thickness, field overlap, and image background on these disparity tolerances were considered. With these parameters manipulated, the most marked differences in tolerance occurred as a function of the background against which the display images were viewed. The disparity tolerances were significantly lower when the images were viewed against a simulated real world background, compared to a homogeneous visual background. That is, the permissible differences in orientation between corresponding retinal images in the left and right eyes are smaller when the eyes must also attend to a real world background with its articulated visual intelligence. The basis for the visual difficulty is the compensatory eye movements required for alternate visual fusing of the display images and objects in the real world. This phenomenon exists for both horizontal and vertical disparities, but the magnitudes of the differences involved due to the change in background are not the same.

The real world background was a static aerial view in previous studies. This simulation is reasonable for situations involving high-altitude flight and no appreciable rates of change of attitude or heading. However, since the real world background has been found important for binocular disparity tolerances, questions regarding the effects of a dynamic background characteristic of flight at low altitudes were raised. The present research was conducted to answer these questions.

Two additional areas involving the application of head-up displays in helicopters were investigated in this program. The first involved the extent to which stereopsis is a factor in the perception of distance from the cockpit. At the combinations of speed and altitude at which fixed-wing aircraft operate, and with the relatively shallow cockpit cutoff angles for these aircraft, there is little likelihood that stereoscopic vision is a factor in the perception of depth or range by the pilot. However, at the slow speeds, low altitudes, and steep viewing angles which are operationally important to helicopter pilots, stereopsis may well play a significant role in the pilots' perception of the real world from the cockpit. If so, the compatibility of collimated head-up display imagery viewed binocularly with near vision of the ground must be established.

The second area involved the helicopter flight regime which permits ground tracks that can differ appreciably from the heading of the aircraft, and climb and dive angles

that differ from the pitch attitude of the vehicle. Its regime is in sharp contrast to that of the fixed-wing aircraft, where the relatively small differences between ground track and heading are due to drift angle, and, for short time periods, yaw angle. In elevation there are similarly small differences between pitch and flight path angle. These considerations indicate that head-up displays for helicopters may require a different range of field coverage from fixed-wing installations. A study to determine the required fields of view for helicopter head-up displays was therefore also undertaken as part of this report.

BINOCULAR DISPARITY STUDIES

Modifications to Research Apparatus

The telecentric viewing system designed and fabricated in previous studies (Phase I) (1) was suitable for studying dynamic head-up display imagery viewed against a static real world background. The series of binocular disparity studies planned for this effort (Phase II), however, required viewing these dynamic images against a moving real world background, typical of high-speed flight at low altitudes. This new requirement dictated modifications to the viewing apparatus. Projected motion pictures were selected as the best choice for incorporating a moving view of the real world in telecentric viewing equipment. The optical and electronic schemes for projecting and synchronizing these motion pictures with the head-up display imagery are described in the following paragraphs.

Optical System

The basic viewing system used in Phase I is shown schematically in Fig. 1. The device is an optical system designed on the principles of on-axis viewing through twin telecentric units. Each eye is provided with an identical viewing system so that even an extremely small distortion, if it should occur, is identical for both eyes and therefore will not generate any binocular disparity. Further precision is obtained by having both systems view a common object, the cathode ray tube. Hence, there is no problem concerning the accuracy of object replication for the two viewing systems.

The viewing system functions in the following manner. For right-eye viewing, the light from a display symbol present on the CRT face is transmitted through a prism beam splitter, totally reflected by mirror M_{R1}, collected by lens L_{R1}, and totally reflected by mirror M_{R2}. The light is then converged by lens L_{R2}, passes through aperture stop AS_R and shutter S_R, diverges, and is collected by lens L_{R3}. After total reflection by mirror M_{R3}, an image is formed in the plane of field stop FS_R. This image is viewed by the right eye after it is collimated by lens L_{R4}, and reflected by the half-silvered mirror M_{R4}. Light from the CRT reaches the left eye through the left half of the system in a comparable manner. Interpupillary distance is adjusted by moving mirrors M_{L4} and M_{R4} in unison, forward or aft. The subject's head position for viewing is stabilized with a chin and head support.

The field of view is determined by field stops FS_{LR}, FS_R, and FS_L. FS_{LR} is common to both eyes, while FS_R and FS_L affect only the fields for each of the eyes. Alternate presentations are made to the eyes by proper phasing of shutters S_R and S_L. The two shutters are driven by a common motor through a timing belt and geared pulley arrangement. Luminance matching of the two systems is accomplished by inserting appropriate neutral density filters near lenses L_{R1} and L_{L1}. Aperture and field stops can be varied in discrete steps. The optical characteristics of the system produce an overall magnification of unity.

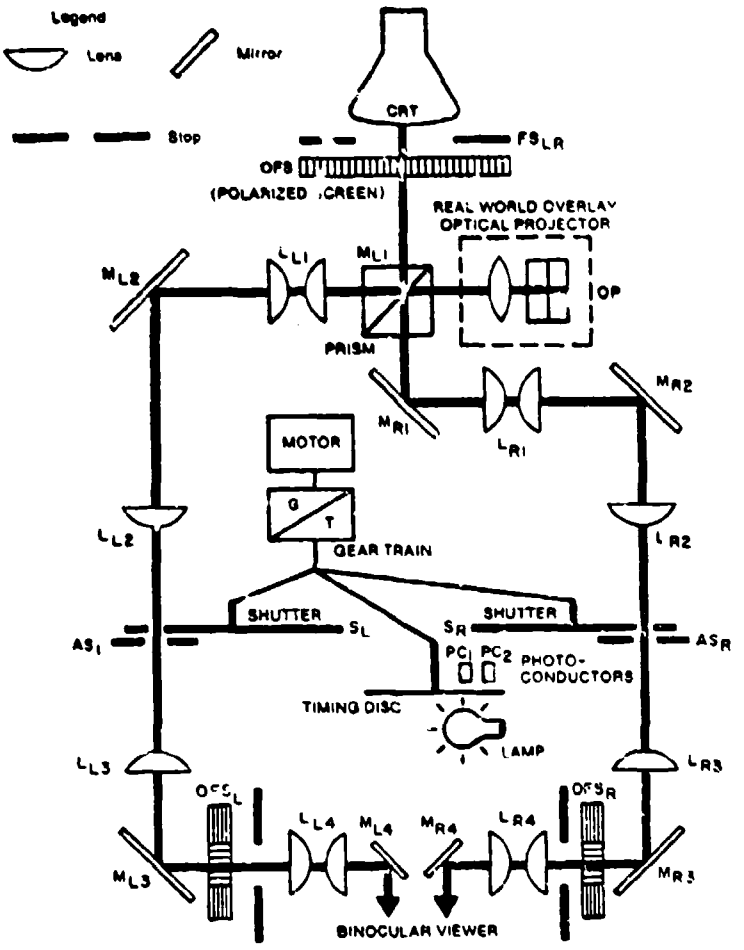

Fig. 1—Optical schematic of telecentric viewing system

Binocular disparities are obtained by presenting disparate images on the CRT to the two eyes alternately at a frequency above flicker fusion. Disparate CRT images are generated by inserting X and Y displacements of the displayed images into one of the sequential fields. The shutters are synchronized so that one eye views the images in an undistorted field, while the other eye sees the distorted field only.

Binocular overlay viewing is done by an optical projection (OP) system which transmits the static image of a 35-mm color transparency to the two optical channels from the right side of the prism beam splitter. Any reasonable aerial view of real terrain can be used as the static rendition of the real world background.

Dual overlapping monocular fields for the images generated on the CRT are created with polarized screens in front of the face of the CRT at OFS, and OFS_L and OFS_R in the two viewing channels. OFS and OFS_L are cross-polarized for all but a circular central portion of the field, representing one monocular image field in the display. The same cross-polarization is accomplished with both OFS_L and OFS_R. Suitable lateral placement of OFS_L relative to OFS_R will produce the desired dual overlapping fields, as shown in Fig. 2. The circular central portions of OFS_L and OFS_R are polarized in the same direction as OFS, to provide uniform luminance for the real world overlay across the full field.

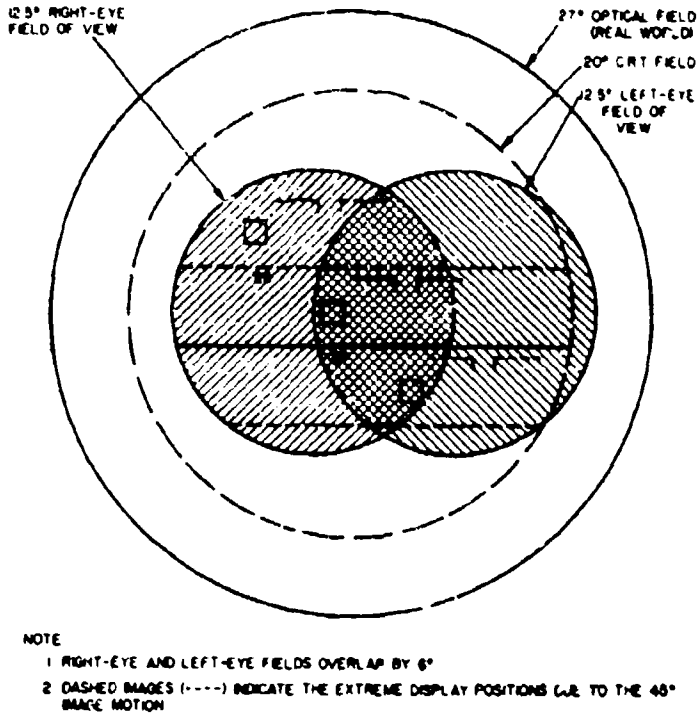

Fig. 2—Modified telecentric viewing system

The moving real world background was introduced by substituting a 16-mm motion picture projection system for the simple optical projector (OP) in Fig. 1. The resulting system is shown in Fig. 3. The image projected by the 16-mm projector, a Graflex Model 920R sound unit, is transmitted through an entrance pupil to the system at the prism P by the optical relay. The relay serves two purposes. It provides an optical path from the projector to the viewing system consonant with the permissible placement of the projector, and it orients the image from the projector for correct viewing by the observer. The image is transmitted by the set of four relay lenses, L_{OR1}, L_{OR2}, L_{OR3}, and L_{OR4}. The mirror M_{OR1} provides both a 90-degree bend in the optical path and a required left-right lateral image reversal. The Dove prism P_{OR1} inverts the image. The combination of M_{OR1} and P_{OR1} effectively provide a required 180-degree rotation of the image about the optical axis of the relay system.

The 16-mm motion pictures used in the projector were copies of film made during flight at low altitudes for use in the JANAIR Studies of Geographic Orientation (2,3). The lens used in the camera had an extremely short focal length (5.7 mm), which provided a wide-angle coverage of about 96 degrees diagonally on standard 16-mm film. The angular field available to the real world background in the viewing system is 26 degrees. If the 16 mm film was projected with a 1.0 magnification to simulate the altitude of the aircraft in which the motion pictures were taken, only a small central portion of the film would be presented in the field of view, revealing the grain of the film in the display. This was demonstrated in a preliminary optical arrangement. The configuration which was adopted involved a 50-mm projection lens and a magnification factor of 2.52 for the relay. The projection lens reduced the material on the film to the ratio 5.7 mm/50 mm, and the relay increased this value to 0.287. This configuration used a sufficient portion of each film frame to provide a suitably fine-grained image in the viewing system. However,

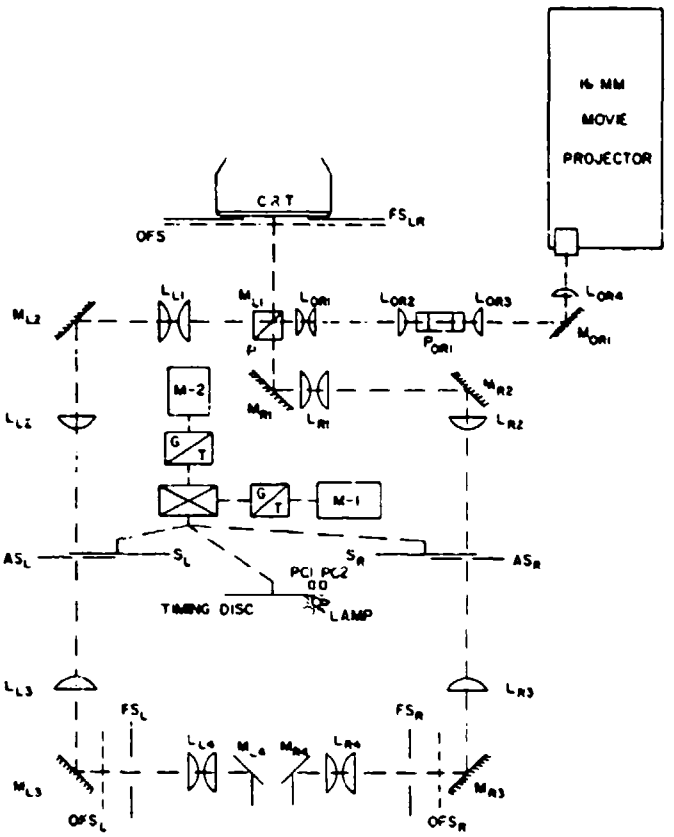

Fig. 3—Dual overlapping monocular fields

the apparent altitude displayed for the subjects was increased by the ratio 1/0.287, or about 3.5 times the picture taking altitude.

Synchronization System for Display and Background

The head-up display system used in these studies is identical to the display in Phase I (1). A display generator provides four typical flight information images and presents them on the CRT in the viewing equipment. These are a horizon line, a flight path marker, a square and a two-digit numeral, as shown in Fig. 2. The images may be fixed, to form a static display, or continuously varied in position to form a dynamic display. The display generator is triggered by synchronization pulses from the shutter timing disk. The position of the display images for either eye are displaced within the display generator by changing the gains and offsets of the CRT deflection amplifiers from one set of values to another during alternate display presentations. Due to the synchronization between the display and the shutters, the eyes see two displays with a controlled relative placement. The visual effect is that of binocular disparity.

The introduction of a moving real world background through the medium of motion pictures required synchronizing the visual consonance between the intermittent head-up display and the background. Complete synchronization between the two media, in both frequency and phase, was considered essential to ensure that there would be no effects on

visual comfort introduced by the equipment. Standard 16-mm sound film is taken at 24 frames per second, and projected at 48 frames per second, each frame being presented twice by the rotary shutter in the projector. The 48-Hz frame rate was therefore considered basic to the head-up display image rate of 24 frames per second for each eye.

The timing requirements for the operation of the motion picture projector, the display images, and the shutters in the viewing system are shown graphically in Fig. 4. The successive projected motion picture frames are alternately presented to the left and right eyes by the synchronization of each frame with the corresponding shutter in the viewing apparatus. The head-up display images are presented to each eye at the same time by the initiating trigger pulse generated by the timing disk, which is mechanically synchronized with the shutters (Fig. 3). The disparity synchronization pulse assures that each of the display images are appropriately placed on the CRT to provide the disparate images to the eyes.

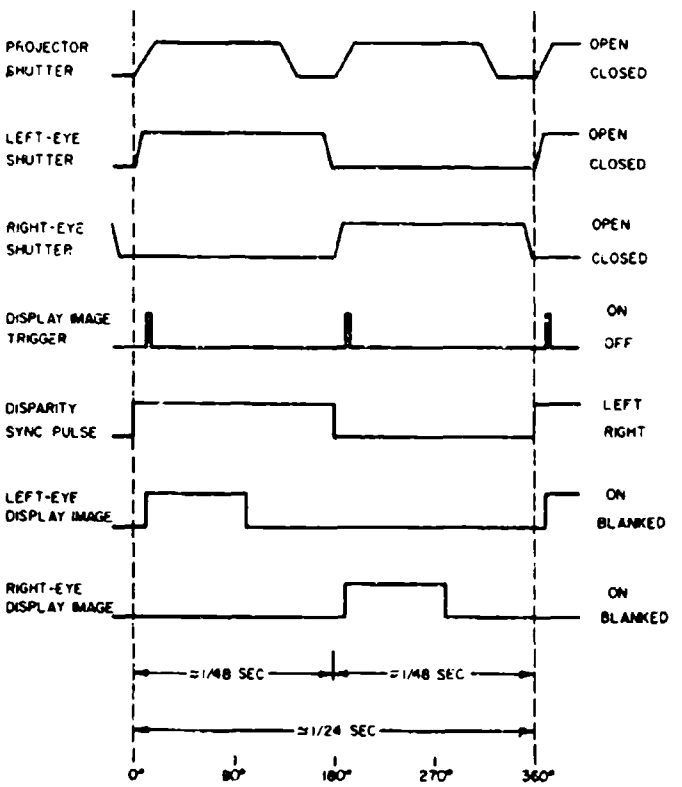

Fig. 4—Timing diagram for synchronization of viewing system

The synchronization between the motion pictures and the display imagery was accomplished by modifying the drive system in the viewing apparatus as shown in the block diagram in Fig. 5. The drive action for the viewing system is accomplished in the following manner. The main drive power is supplied by a 400-Hz synchronous motor which has a speed of 12,000 rpm. The gear reduction between this motor and the shutters in the

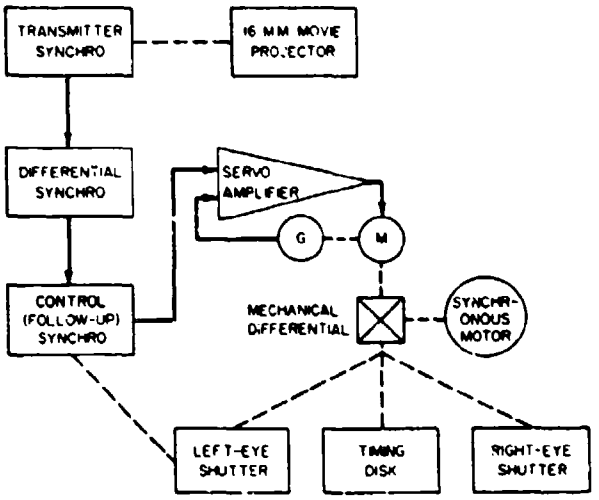

Fig. 5—Block diagram of synchronized drive system

viewing system is 8.33:1, so that the shutters operate at a nominal speed of 1440 rpm, or 24 revolutions per second. Synchronization with the motion picture projector is implemented by a servo motor, which also has an input to shutter motion through the mechanical differential. The servo motor is controlled by a closed-loop, synchro followup system. A transmitter synchro is mechanically coupled to the shutter mechanism in the projector, and a control transformer is coupled to the shutter system in the viewing equipment. The output from these synchro units feeds the servo amplifier controlling the servo motor to maintain the same positional relationship between the shutters in the projector and the viewer. In addition, a differential synchro, mounted on the experimenter's control panel, is electrically interposed between the transmitter and control synchros, which permits manual adjustment of the phase between the shutter systems. The servo motor system permits a modification of the primary shutter drive speed of 60 rpm, or 1 revolution per second, to accommodate the speed of the motion picture projector.

Design and Conduct of Experiments

Experimental Design

The binocular disparity studies were planned for six test pilots, three from the U.S. Army and three from the U.S. Navy. Two of the Army pilots had recently completed their fixed-wing training, while the third was an experienced helicopter pilot. The Army pilots were all provided by the U.S. Army Aviation Center at Fort Rucker, Alabama. The Navy pilots were from the Naval Air Test Center, Patuxent River, Maryland. They were all test pilots, and one of these, from the Marine Corps, had some flight experience with a head-up display. The first two Army pilots (designated A1 and A2) had not been given detailed optometric examination to determine their phorias (relative orientation of the eyes without fixation) and ductions (movement of the eyes to maintain visual fusion). It was assumed that the Ortho-Rater examinations they had been given in service were sufficient to qualify them as test subjects. However, the next two Army pilots provided unusual contrasting data in preliminary disparity experiments to warrant further examination by the optometrist at Sperry. One subject had unusually high ductions so that he could readily compensate for large binocular disparities without experiencing any significant

visual discomfort. The second had a large esophoria, without sufficient reserve duction, so that visual discomfort was easily induced after short periods of testing. These subjects were therefore not given the full experimental regimen, and their test data were not included in the study. All four subsequent subjects (A3, N1, N2, and N3) were examined by the optometrist, and the results are summarized in Table 1.

Table 1
Results of Maddox Rod Test for Phorias and Ductions of Subjects for Distant Vision

Subject	A3		N1	N2		N3	Normal Range
Date	9-22-69	9-29	10-6	10-20	10-21	1-6-70	
Phorias—in prism diopters							
Lateral	0	1/2 EXO	1 EXO	4 ESO	5 ESO	1/2 EXO	0-1 EXO, ESO
Vertical	0	0	0	0	0	0	
Ductions—in prism diopters break/recovery							
Induction	8/6	20/8	11/6	22/16	28/20	16/14	19/10
Outduction	5/3	6/4	7/4	2/0	4/2	8/5	7-9/5
Supraduction	3/2	3/2	3/1	1/0	1/0	3/2	3/2
Subduction	2/1	4/2	3/1	1/0	2/1	3/2	3/2
Refractive Errors —in diopters	OU	+0.75	OD+0.50 −1.25 cyl × 95 OS to 0.25 −1.25 cyl × 90	OU	+1.00	OU+1.00 −0.25 cyl × 180	0 to +1

Notes (from Ref. 4):
1 prism diopter = $\tan^{-1} 0.01$ = 10 nirod
OD — oculus dexter — right eye
OS — oculus sinister — left eye
OU — oculi uniter — both eyes

The experiments were designed to measure visual performance with the head-up display images viewed against a dynamic real world background, as functions of the following parameters:

- Brightness of images
- Image motion
- Line thickness of images
- Real world background
- Overlapping monocular fields

These primary variables were also investigated in the Phase I studies, in which both a static scene of the real world and a homogeneous field with uniform luminance were used as backgrounds.

Seven test conditions were established based on these variables and are summarized in Table 2. The first six of the test conditions are counterparts of the correspondingly numbered test conditions in Phase I. The letter A has been added to the designation to distinguish the tests in Phase II. The seventh condition (15A) has been added to cover the effect of pure vertical motion of the display images. Condition 1A is a reference

Table 2
Summary of Binocular Disparity Test Conditions

Test Condition	Image Motion				Image Brightness		Line Thickness		Display Field	Number of Sessions						
	Oblique (45°)	Horizontal	Vertical	Static	High	Low	Fine	Thick	Full Binocular	Overlapping	Pilot A1	Pilot A2	Pilot A3	Pilot N1	Pilot N2	Pilot N3	Totals
1A	●				●		●		●		3	3	3	3	3	3	18
2A		●			●		●		●		3	3	2	3	3	2	16
3A				●	●		●		●		3	3	3	3	3	3	18
4A	●					●	●		●		3	3	4	3	3	3	19
5A	●				●			●	●		3	3	2	3	3	3	17
8A	●				●		●			●	3	3	4	3	3	3	19
15A			●		●		●		●		3	3	2	3	3	3	17
Totals											21	21	20	21	21	20	124

condition in which there is an oscillation of the images in a direction at 45 degrees from the vertical with bright, fine line images. Condition 2A involves the same images moving in a horizontal oscillation, while the images are static in Condition 3A. Images with low brightness were used in Condition 4A. The normal brightness of the images involved a liminance ten times the luminance of the brightest region in the real world background. For the low-brightness condition, the luminance of the images were reduced to one-tenth of its normal value. Images with thick lines were displayed in Condition 5A. The standard (fine) line width of the images was 2.4 minutes of arc which was increased to 6 minutes to represent thick lines. Dual overlapping monocular fields were presented to the subjects in Condition 8A (Fig. 2). In this situation, the right eye sees the circular field shown to the left in Fig. 2, while the left eye sees the same type of field shown to the right. The overlapping region in the center is seen binocularly. Each monocular field has a maximum horizontal extent of 12.5 degrees, while the extent of the overlap is 6 degrees. Condition 15A introduced pure vertical motion of the images in lieu of the oblique motion used as a standard in other conditions.

The disparity levels used in the tests were generally the same as in Phase I. However, for some subjects, it was necessary to increase these to produce significant manifestations of visual discomfort in their test responses. Schedules in which horizontal disparities were doubled and trebled (2X and 3X), and in which vertical disparities were doubled, were therefore also generated. Compilations of the disparities used in the tests are presented in Table 3.

The changes in the dynamic visual background made it desirable to replicate the various test exposures of the subjects with the same sets of visual scenes. This procedure would minimize any variability in the results which may be introduced by the background. Magnetic striping for sound recording was therefore provided on one edge of the 16-mm film. The motion picture projector could play back sound of this type of magnetic recording. Voice commands for the test subjects' exposures to the displays and responses were recorded on the film so that replicated background stimuli were assured. The timing of the trials for the duration of each reel of projected film was also controlled by this technique.

Table 3
Binocular Disparity Levels Used in Test Schedule

1X		2X		3X		
Dial Setting	Horizontal Disparity (minutes)	Dial Setting	Horizontal Disparity (minutes)	Dial Setting	Horizontal Disparity (minutes)	
530	-18	560	-36	590	-54	Esophoria (convergent) (near)
520	-12	540	-24	560	-36	
510	- 6	520	-12	530	-18	
505	- 3	510	- 6	515	- 9	
500	0	500	0	500	0	Orthophoria
495	+ 3	490	+ 6	485	+ 9	Exophoria (wall-eye) (far)
490	+ 6	480	+12	470	+18	
485	+ 9	470	+18	455	+27	
480	+12	460	+24	440	+36	

1X		2X		
Dial Setting	Vertical Disparity (minutes)	Dial Setting	Vertical Disparity (minutes)	
520	+12	540	+24	Hyperphoria (right eye high)
515	+ 9	530	+18	
510	+ 6	520	+12	
505	+ 3	510	+ 6	
500	0	500	0	Orthophoria
495	- 3	490	- 6	Hypophoria (right eye low)
490	- 6	480	-12	
485	- 9	470	-18	
480	-12	460	+24	

Test Procedures

Each test, representing a horizontal or a vertical disparity experiment under a particular set of display conditions selected from Table 2, involved ten replications of each of nine disparity levels from Table 3, or a total of 90 data points. The disparity levels were presented in a random sequence to the test subjects. If both horizontal and vertical disparities for each display condition are considered, a full test session included 180 data points.

The experiments were conducted as follows: The interpupillary distance of a subject was measured, and the spacing of the two exit pupils in the binocular viewing apparatus was adjusted accordingly. The subject was then seated in the viewing compartment and his head rest and seat were adjusted to provide a comfortable viewing condition. The subject became adapted to the low level of ambient illumination and final adjustment of the interpupillary setting of the apparatus was made.

The sequence of operations for each trial, determined by the commands on magnetic tape, was as follows: On the first run, the command "READY, ONE" was given to the test subject to alert him to the start of the trial. Five seconds later, the subject was told to begin viewing the display, following the moving square image, by the verbal command "MARK." After 15 seconds of exposure to the display situation, the subject responded to the command "READ" by rating his level of visual comfort in one of six response

c. ries. This novel measure of visual performance relating to binocular disparity was est..lished in Phase I as a result of the following considerations. Tolerance for disparities is usually associated with the ability of an observer to retain single vision, i.e., to prevent visual doubling of objects or displays. However, in preliminary experiments in Phase I, subjects complained of visual stress and annoyance caused by disparities that are considerably smaller than those that produce doubling. Therefore, a psychometric rating system was required to measure visual stress levels at disparity levels for which single vision exists, as well as for doubling phenomena. The rating scale which was developed consists of the six categories:

Response Category	Visual Comfort Level	
1	Excellent	Comfortable
2	Comfortable, short of excellent	
3	Mildly uncomfortable	Uncomfortable with single vision
4	Severely uncomfortable	
5	Doubling less than 50 percent of the time	Double vision
6	Doubling more than 50 percent of the time	

On this basis, categories 1 and 2 represent two levels of comfortable vision, while categories 3 and 4 provide for two levels of discomfort, all with single vision. Image doubling is covered by categories 5 or 6, depending on the persistence of the doubling.

Fifteen seconds after the "READ" command, the second trial was initiated with the verbal alert "READY, TWO," and the procedure was repeated. The experimenter recorded the verbal response of the subject to each trial, and set the appropriate disparity for each trial in the control panel. A reel of motion picture film permitted 30 trials, after which the subject was given a brief rest while the film was being rewound prior to initiating a new set of 30 trials.

Each session under a given set of conditions covered 180 data points, 90 for horizontal disparities and 90 for vertical disparities. The experimental design involved three replications of each of the seven test conditions with each subject. Two weeks of each subject's time were required, considering optometric examination, pretest indoctrination, and the 21 sessions planned. A summary of the data obtained for each of the six test subjects is included in Table 2.

Data Reduction and Analysis

Data Reduction

The volume of data accumulated in the binocular disparity studies and the number of numerical analyses to be performed with these data were both large. Therefore, computer handling of this information was planned. A Univac 1108 system was used to perform the computations, and a Cal-Comp Model 763 performed the digital plotting automatically, using the tape output from the computer.

Each test session yielded 90 data points for horizontal disparities and 90 data points for vertical disparities. A total of 124 individual sessions were accomplished with the six test subjects, distributed among test conditions as shown in Table 2. Time limitations

VISUAL REQUIREMENTS FOR HEADS UP DISPLAY

CONDITION 1A STANDARD SET 1
PILOT A1

HORIZONTAL DISPARITY STIMULUS RANGE 1X

COMFORT LEVEL	530	520	510	505	500	495	490	485	480
	MINUTES OF ARC								
	-18	-12	-6	-3	0	3	6	9	12
1	6	4	3	6	4	2	2	0	0
2	0	2	6	3	5	3	4	0	0
3	2	4	1	1	1	3	2	1	0
4	2	0	0	0	0	0	2	1	1
5	0	0	0	0	0	2	0	7	1
6	0	0	0	0	0	0	0	1	8
SUM	10	10	10	10	10	10	10	10	10
% ROWS 12	60	60	90	90	90	50	60	0	0
% ROWS 123	80	100	100	100	100	80	80	10	0

COMFORT LEVEL 2 = 6.50 MIN. OF ARC
COMFORT LEVEL 3 = 6.00 MIN. OF ARC

ESO EXO

VERTICAL DISPARITY STIMULUS RANGE 1X

COMFORT LEVEL	480	485	490	495	500	505	510	515	520
	MINUTES OF ARC								
	-12	-9	-6	-3	0	3	6	9	12
1	0	0	1	5	4	4	4	0	1
2	0	0	1	3	5	4	3	3	0
3	0	0	4	1	1	2	2	3	3
4	0	2	1	1	0	0	1	4	0
5	1	5	3	0	0	0	0	0	4
6	9	3	0	0	0	0	0	0	2
SUM	10	10	10	10	10	10	10	10	10
% ROWS 12	0	0	20	80	90	80	70	30	10
% ROWS 123	0	0	60	90	100	100	90	60	40

COMFORT LEVEL 2 = -4.50 MIN. OF ARC 7.50 MIN. OF ARC
COMFORT LEVEL 3 = -4.00 MIN. OF ARC 7.00 MIN. OF ARC

HYPO HYPER

Fig. 6—Computer printout of reduced disparity data

prevented accomplishing three replications of each condition with all the pilots. The data were tabulated by the experimenter while conducting the tests, and entered on computer punch cards for machine processing.

Each set of 90 data points is distributed among the nine levels of disparity (Table 3) with 10 points per disparity as shown in the matrices in the sample computer printout sheet in Fig. 6. For each disparity level in each matrix, the percentage of the responses that were equal to or better than response category 2, and equal to or better than response category 3, were determined. These are designated as % rows 12 and % rows 123 in Fig. 6. If these cumulative percentages are plotted as a function of disparity level, two curves similar to Fig. 7 are obtained for each matrix. The lower curve through the plotted points in the circles represents the variation of the sum of response categories of 2 or better, i.e., plus 2, as a function of disparity level. The upper curve through the points with the crosses represents the response categories of 3 or better, i.e., plus 2 plus 3.

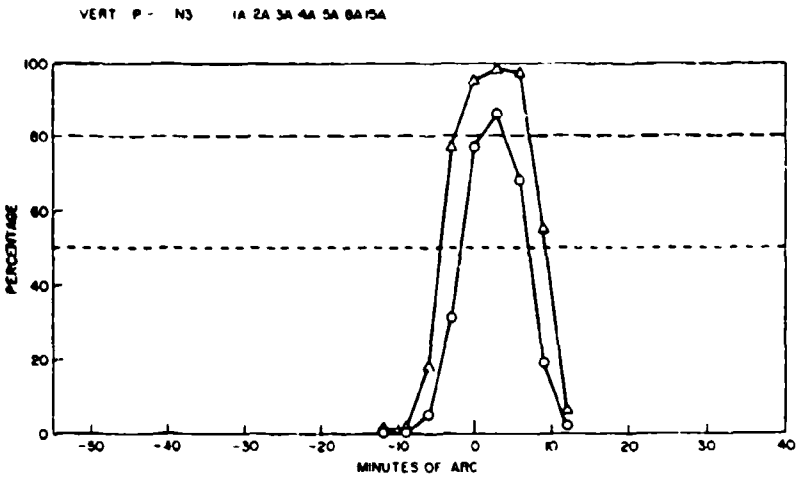

Fig. 7--Digitally generated plot of reduced disparity data

Families of curves similar to Fig. 7 summarize the variation in visual performance as a function of horizontal and vertical disparity levels. To apply these data to the optical design problem for head-up displays, maximum permissible disparities must be established. These in turn depend on minimum acceptable visual performance levels.

The same criteria used in Phase I, namely,

- Comfortable vision or better (Categories 1 or 2) 50 percent of the time, designated Comfort Index 2
- Mild discomfort or better (Categories 1, 2, or 3) 80 percent of the time, designated Comfort Index 3,

applied to these studies. It was judged that a head-up display that met these criteria based on the data for sustained 15-pound viewing would be satisfactory in real flight.

The binocular disparities associated with each of these comfort indices were determined for each set of matrices, as indicated in Fig. 6. These are shown in minutes of arc under each matrix, identified as comfort level 2 and comfort level 3. They represent the

disparities at the intersections of the horizontal line at 50 percent with the lower curve and the intersections of the horizontal line at 80 percent with the upper curve (Fig. 7).

The data reduction shown in Fig. 6 was accomplished for all pilots, test conditions, and test sessions, individually and in various combinations. First, the data for the 124 individual test sessions were reduced. The binocular disparities for comfort indices 2 and 3, from these data, are presented in Table 4. For each test session the lowest of these two values of vertical disparity, exophoric (diverging, far) horizontal disparity, and esophoric (converging, near) horizontal disparity in Table 4 were selected, and these are summarized in Table 5.

The foregoing process was repeated with the data for replicated sessions combined, yielding 42 combinations of pilots and test conditions. The results are summarized in Table 6. The analysis was then extended to various combinations of test conditions for each of the six test subjects. Conditions 1A, 2A, and 15A, which cover oblique, horizontal, and vertical image motions with the same levels of image brightness and line thickness, were first combined. Then Conditions 4A and 5A, representing images with low brightness and thick lines, were combined. The reference Condition 1A was then added to 4A and 5A. Then all conditions except 8A, the display with dual overlapping monocular fields, were merged. And, finally, all seven test conditions were combined. The resulting critical binocular disparity levels for each of the pilots are presented in Table 7.

All of the preceding pooling of data maintained isolation among the data from the different pilots, so that differences among the pilots would not confound possible differences introduced by the test conditions. For final pooling of data, the Army pilots were combined (A1, A2, A3), the Navy pilots were combined (N1, N2, N3), and then all six pilots were combined. This was accomplished for each of the seven individual test conditions, and the various combinations of test conditions. In combining data for different groups of pilots, the differences in stimulus ranges used for various pilots (Table 3) preclude direct superposition of the data matrices. Therefore, the following procedure was used. In the relatively few instances where extended stimulus ranges were employed, the values for the responses corresponding to standard (IX) stimuli were determined by interpolation between experimental data points. Then, the response plots for groups of pilots were generated from the resulting data by weighting each of the pilots equally. Critical disparity levels were determined from these plots, and these are included in Table 7.

The comfort level curves for the six pilots under seven different conditions (42 combinations) and the five combined sets of conditions (30 combinations) were plotted by the Cal-Comp digital plotter. These represent 144 curves, 72 each for horizontal and vertical disparities.

Statistical Analyses

Statistical analyses were used to determine whether there are any differences in binocular disparity tolerances among test conditions and among pilots. Analysis of variance techniques are useful in obtaining answers to these questions. Conventional parametric analyses could not be appropriately applied to these data since the assumption of normality in the distributions could not be supported. Nonparametric statistical tests are more suitable under these circumstances.

First, consider possible differences in performance among the seven test conditions, taking the data obtained for each of the six pilots under these conditions (Table 6). The Friedman Two-Way Analysis of Variance by Ranks (5) was selected to determine if the

Table 4
Binocular Disparity Tolerances for Individual Test Sessions

Pilot A1

Session No.	Set No.	Condition	Comfort Index 2				Comfort Index 3			
			Horizontal Disparity (minutes)		Vertical Disparity (minutes)		Horizontal Disparity (minutes)		Vertical Disparity (minutes)	
			Near	Far	Rt. Eye Low	Rt. Eye High	Near	Far	Rt. Eye Low	Rt. Eye High
1	1	1A	↑	6.50	4.50	7.50	↑	6.00	4.00	7.00
2	1	3A	↑	1.80	2.40	7.50	↑	3.43	3.37	6.00
3	1	15A	↑	4.50	4.87	7.00	↑	3.75	3.86	6.86
4	1	8A	↑	7.00	4.50	7.50	↑	6.00	5.00	7.20
5	1	4A	↑	5.00	4.00	4.80	↑	4.50	3.86	7.00
6	1	5A	12.00	4.50	4.20	5.25	↑	5.00	4.50	6.00
7	1	2A	10.00	2.40	2.25	6.86	16.00	3.60	3.37	6.86
8	2	2A	↑	3.00	1.50	4.87	↑	3.60	3.00	5.00
9	2	5A	↑	3.00	2.50	4.80	↑	4.00	3.37	6.00
10	2	4A	16.00	4.50	4.20	6.00	↑	3.60	3.86	6.50
11	2	8A	↑	7.29	5.14	7.00	↑	6.75	6.00	7.00
12	2	15A	↑	2.50	3.60	6.60	↑	3.37	3.43	6.00
13	2	3A	16.00	5.14	4.50	4.50	↑	6.00	3.67	6.00
14	2	1A	↑	4.20	1.67	6.00	↑	3.00	2.00	4.50
15	3	1A	↑	2.50	3.60	6.86	↑	1.50	2.00	6.00
16	3	3A	15.00	4.87	3.50	4.71	↑	4.20	3.67	3.60
17	3	15A	↑	3.50	3.50	5.00	↑	3.43	1.50	4.20
18	3	8A	↑	4.50	3.86	7.50	↑	3.60	3.43	6.75
19	3	4A	↑	2.40	3.00	4.71	↑	3.37	2.00	5.00
20	3	5A	↑	1.50	2.14	4.67	↑	2.00	1.50	5.00
21	3	2A	15.00	4.00	3.86	4.71	↑	4.50	3.42	5.00
Pilot A2										
1	1	1A	15.00	6.00	6.00	7.12	15.00	10.00	7.20	7.00
2	1	3A	6.00	6.00	4.12	3.00	5.00	9.00	4.00	3.75
3	1	15A	10.00	5.40	3.75	5.00	9.00	5.00	4.00	5.00
4	1	8A	8.00	5.85	6.00	4.50	0.00	4.50	4.50	6.43
5	1	4A	9.00	2.00	↓	3.50	12.00	3.00	3.00	3.75
6	1	5A	1.00	1.00	2.40	1.71	12.86	3.00	3.00	3.00
7	1	2A	↓	3.00	1.50	2.00	3.75	6.00	3.86	3.00
8	2	2A	3.00	4.50	3.86	1.80	6.00	5.00	3.75	3.43
9	2	5A	0.00	0.00	1.50	3.00	6.00	0.00	3.37	3.00
10	2	4A	3.60	3.75	↓	3.75	8.00	3.00	3.33	1.50
11	2	8A	3.00	0.00	0.75	1.50	6.00	1.00	3.00	0.00
12	2	15A	3.00	0.00	3.75	1.50	4.00	6.00	4.00	5.00
13	2	3A	0.75	0.60	3.00	1.00	6.00	2.00	3.00	3.60
14	2	1A	1.00	0.75	0.00	3.00	12.86	6.00	3.75	3.00
15	3	4A	6.00	↓	1.20	1.00	9.00	3.00	2.00	4.50
16	3	2A	↓	↓	↓	↓	7.00	3.60	3.00	3.00
17	3	8A	↓	↓	↓	↓	4.50	9.00	↓	9.00
18	3	5A	↓	↓	↓	↓	3.00	1.00	0.60	0.75
19	3	15A	↓	↓	↓	↓	4.50	3.00	3.00	3.00
20	3	1A	↓	↓	↓	↓	4.50	↓	0.00	0.00
21	3	3A	↓	↓	↓	↓	8.00	↓	↓	6.00

Table 4 continues

Table 4 (Continued)
Binocular Disparity Tolerances for Individual Test Session

Pilot A3

Session No.	Set No.	Condition	Comfort Index 2				Comfort Index 3			
			Horizontal Disparity (minutes)		Vertical Disparity (minutes)		Horizontal Disparity (minutes)		Vertical Disparity (minutes)	
			Near	Far	Rt. Eye Low	Rt. Eye High	Near	Far	Rt. Eye Low	Rt. Eye High
1	1	15A	↑	9.00	8.00	9.00	↑	↑	9.43	11.00
2	1	8A	↑	↑	↑	↑	↑	↑	↑	↑
3	1	4A	↑	15.00	↑	↑	↑	14.40	↑	↑
4	1	5A	↑	16.29	14.67	15.75	↑	19.33	14.00	18.75
5	1	2A	↑	15.00	9.00	15.00	32.00	14.40	10.00	13.20
6	2	2A	33.60	15.33	9.33	12.00	↑	14.40	7.71	13.20
7	2	5A	34.00	13.20	10.29	15.00	32.00	14.40	10.00	14.00
8	2	4A	30.00	10.29	13.71	14.67	↑	13.33	13.20	14.00
9	2	8A	↑	19.00	15.00	16.29	↑	19.71	14.00	18.67
10	2	15A	28.00	14.57	10.29	15.00	26.00	13.50	9.00	13.50
11	1	3A	24.00	11.00	9.33	14.67	28.00	13.00	10.00	13.33
12	1	1A	30.00	15.00	9.00	15.00	30.00	13.71	8.00	13.50
13	2	3A	30.86	13.71	9.75	13.71	27.00	13.50	10.00	13.50
14	3	4A	↑	13.00	9.75	14.67	↑	13.71	13.20	18.00
15	2	1A	31.20	14.67	9.43	14.67	28.80	15.00	13.20	13.71
16	3	8A	↑	16.29	12.00	14.67	↑	18.75	13.50	18.00
17	4	8A	27.00	15.43	11.00	15.00	↑	16.00	13.71	16.00
18	3	1A	24.00	12.00	9.33	15.00	27.43	13.33	13.20	14.00
19	4	4A	28.80	13.00	11.00	14.67	↑	12.75	12.86	16.00
20	3	3A	19.50	9.75	8.67	10.29	24.00	12.86	12.00	13.50
Pilot N1										
1	1	1A	18.00	19.50	7.71	12.00	30.00	21.00	6.75	12.67
2	1	3A	11.57	12.00	6.00	10.00	13.50	18.00	7.20	12.67
3	1	15A	6.43	15.00	7.71	8.00	20.57	13.50	7.33	12.75
4	1	8A	0.00	9.00	7.00	↓	18.00	24.00	6.86	12.00
5	1	4A	↓	18.00	0.00	6.00	12.00	15.00	6.67	7.50
6	1	5A	3.37	6.75	3.00	3.00	18.00	18.12	8.00	11.00
7	1	2A	↓	9.00	↓	7.20	18.00	15.00	6.37	10.00
8	2	2A	2.25	9.00	↓	12.00	36.00	18.00	8.00	12.00
9	2	5A	0.00	14.40	7.50	↑	21.60	18.00	7.50	↑
10	2	4A	3.00	12.00	3.00	5.00	21.00	10.80	6.00	9.86
11	2	8A	0.00	15.00	↓	6.00	25.20	22.50	7.20	↑
12	2	15A	2.25	14.14	1.80	4.80	24.00	15.00	6.75	10.00
13	2	3A	0.00	18.00	↓	4.50	21.60	18.00	5.00	11.00
14	2	1A	1.80	18.00	0.00	3.00	18.00	18.00	6.50	11.00
15	3	1A	1.80	18.00	4.50	0.00	18.00	19.20	6.37	10.00
16	3	3A	↓	19.80	1.50	9.00	13.50	15.00	6.00	10.20
17	3	15A	2.25	18.00	5.00	10.71	26.20	18.00	6.00	10.00
18	3	8A	6.75	18.00	4.50	9.86	22.50	18.00	6.75	11.00
19	3	4A	4.50	23.40	5.25	10.00	15.00	19.80	5.00	11.00
20	3	5A	11.25	21.00	0.00	7.80	18.00	18.00	6.43	↑
21	3	2A	4.50	22.50	3.86	9.60	15.00	20.00	3.86	10.20

Table 4 continues

Table 4 (Continued)
Binocular Disparity Tolerances for Individual Test Sessions

Pilot N2

Session No.	Set No.	Condition	Comfort Index 2				Comfort Index 3			
			Horizontal Disparity (minutes)		Vertical Disparity (minutes)		Horizontal Disparity (minutes)		Vertical Disparity (minutes)	
			Near	Far	Rt. Eye Low	Rt. Eye High	Near	Far	Rt. Eye Low	Rt. Eye High
1	1	1A	8.00	3.00	2.00	6.86	1.50	3.00	3.00	6.75
2	1	3A	10.50	6.00	4.00	6.00	↑	6.00	4.20	6.33
3	1	15A	↓	6.00	3.00	6.60	↑	9.00	4.50	6.50
4	1	8A	3.00	7.00	7.00	3.75	↑	↓	8.00	0.00
5	1	4A	↑	↓	1.00	3.86	↑	3.00	3.50	3.00
6	1	5A	12.00	1.00	0.60	1.50	↑	5.00	2.00	3.75
7	1	2A	0.00	0.00	1.50	3.60	↑	2.00	3.00	3.37
8	2	2A	3.00	↓	3.00	3.00	5.00	↓	3.00	2.00
9	2	5A	4.80	2.00	1.00	1.50	↑	3.00	3.00	1.50
10	2	4A	3.00	↓	↓	↓	12.00	↓	↓	↓
11	2	8A	↓	↓	↓	↓	↓	↓	↓	↓
12	2	15A	↓	↓	0.00	0.00	4.00	↓	↓	↓
13	2	3A	↑	↓	↓	↓	↓	↓	↓	↓
14	2	1A	↓	↓	↓	↓	↓	↓	↓	↓
15	3	4A	4.50	↓	3.00	↓	9.00	0.00	3.37	3.86
16	3	2A	←	↓	↓	↓	12.00	↓	↓	↓
17	3	8A	←	↓	0.00	0.00	0.00	0.00	0.00	3.60
18	3	5A	↓	↓	4.00	6.00	0.00	0.00	3.00	4.00
19	3	15A	0.00	0.00	1.00	3.50	6.00	0.60	0.00	3.60
20	3	1A	12.00	↓	0.00	0.00	↑	↓	3.00	3.00
21	3	3A	↓	↓	↓	3.75	↑	↓	0.00	3.60
Pilot N3										
1	1	1A	13.50	↑	↓	7.20	↑	↑	3.75	6.00
2	1	3A	5.25	4.50	1.00	7.00	13.50	4.00	1.00	9.38
3	1	15A	13.20	6.00	1.29	8.25	14.40	5.00	1.00	8.00
4	1	8A	14.00	7.00	3.50	8.50	15.00	6.00	3.50	8.00
5	1	4A	13.50	4.50	1.00	6.86	16.00	6.37	3.33	7.00
6	1	5A	7.50	6.00	3.00	8.00	13.20	6.00	3.75	9.33
7	1	2A	14.67	3.75	2.25	9.00	14.40	4.00	3.00	9.00
8	2	2A	14.00	2.50	0.75	7.29	14.00	3.50	1.50	7.00
9	2	5A	10.80	2.00	2.14	7.50	13.50	2.00	3.75	8.00
10	2	4A	12.00	1.50	0.00	5.00	14.00	1.50	1.20	6.75
11	2	8A	4.00	1.50	1.80	5.50	6.00	6.00	2.00	7.00
12	2	15A	10.50	2.00	3.00	6.75	14.40	3.00	3.50	7.50
13	2	3A	9.60	4.50	1.88	7.50	13.33	3.00	3.00	8.00
14	2	1A	9.43	4.50	2.25	6.50	13.71	4.20	3.00	7.00
15	3	5A	9.75	5.00	2.40	7.20	13.50	4.00	3.60	7.50
16	3	15A	8.25	5.00	2.14	7.80	13.20	3.75	2.00	9.33
17	3	4A	8.57	4.50	1.80	6.00	12.00	4.00	1.20	6.75
18	3	3A	4.00	3.00	1.80	7.50	7.50	3.00	3.43	6.67
19	3	5A	1.00	1.50	0.00	6.60	3.00	1.50	1.50	6.50
20	3	1A	3.60	2.50	1.88	6.60	6.00	1.20	3.43	6.75

Table 5
Minimal Binocular Disparity Tolerances for Individual Test Sessions

Vertical Disparity (minutes of arc.)														
C / P	1A		2A		3A		4A		5A		8A		16A	
A1	4.00 2.00	1.67	2.25 3.43	1.50	2.40 3.50	3.67	3.86 2.00	3.86	4.20 1.50	2.50	4.50 3.43	5.14	3.86 1.50	3.43
A2	6.00 ↓	0.00	1.50 ↓	1.80	3.00 ↓	1.00	↓ ↓	1.00	1.71 ↓	1.50	4.50 ↓	0.00	3.75 ↓	1.50
A3	8.00 9.33	9.43	9.00	9.33	9.33 8.67	9.75	↑ 9.75	13.20 11.00	14.00	10.00	↑ 12.00	14.00 11.00	8.00	9.00
N1	6.75 0.00	0.00	↓ ↓ 3.86		6.00 1.50	↓	0.00 5.00	3.00	3.00 0.00	7.50	↓ ↓ 4.50		7.33 5.00	1.80
N2	2.00 0.00	↓	1.50 ↓	2.00	4.00 ↓	↓	1.00 ↓	↓	0.60 3.00	1.00	0.00 0.00	↓	3.00 0.00	↓
N3	↓ 1.88	2.25	2.25	0.75	1.00 1.80	1.88	1.00 1.20	0.00	3.00 2.40	2.14	3.50 0.00	1.80	1.00 2.00	3.00
Convergent Horizontal Disparity (minutes of arc.)														
A1	↑ ↑ ↑		10.00↑	↑	↑ 15.00	16.00	↑ 16.00↑		12.00↑	↑	↑	↑ ↑	↑	↑ ↑
A2	15.00 ↓	1.00	↓ 3.00	↓	6.00 ↓	0.75	9.00 6.00	3.60	1.00 ↓	0.00	0.00 ↓	3.00	9.00 ↓	3.00
A3	30.00 24.00	28.80	32.00	33.60	24.00 19.50	27.00	↑ ↑	30.00 28.80	↑	32.00	↑ 27.00	↑ ↑	↑	26.00
N1	18.00 1.80	1.80	↓ 4.50	2.25	11.57 ↓	0.00	↓ 4.50	3.00	3.37 11.25	0.00	0.00 6.75	0.00	6.43 2.25	2.25
N2	1.50 12.00	↓	0.00 ↓	3.00	10.50 ↓	↓	↑ 4.50	3.00	12.00 ↓	4.80	3.00 ↓	↓	↑ 0.00	↓
N3	13.50 3.60	9.43	14.40	14.00	5.25 4.00	9.60	13.50 8.57	12.00	7.50 9.75	10.80	14.00 1.00	4.00	13.20 8.25	10.50
Divergent Horizontal Disparity (minutes of arc.)														
A1	6.00 1.50	3.00	2.40 4.00	3.00	1.80 4.20	5.14	4.50 2.40	3.60	4.50 1.50	3.00	6.00 3.60	6.75	3.75 3.43	2.50
A2	6.00 ↓	0.75	3.00 ↓	4.50	6.00 ↓	0.60	2.00 ↓	3.00	1.00 ↓	0.00	4.50 ↓	0.00	5.00 ↓	0.00
A3	13.71 12.00	14.67	14.40	14.40	11.00 9.75	13.50	14.40 13.00	10.29 12.75	16.29	13.20	↑ 16.29	19.00 15.43	9.00	13.50
N1	19.50 18.00	18.00	9.00 20.00	9.00	12.00 19.80	18.00	15.00 19.80	10.80	6.75 18.00	14.40	9.00 18.00	15.00	13.50 18.00	14.14
N2	3.00 ↓	↓	0.00↓	↓	6.00↓	↓	↓	↓ ↓	1.00 ↓	2.00	↓	↓ ↓	6.00 0.00	↓
N3	↑ 1.50	4.20	3.75	2.50	4.00 3.00	3.00	4.50 4.00	1.50	6.00 4.00	2.00	6.00 1.50	1.50	5.00 3.75	2.00

Table 6
Binocular Disparity Tolerances for Each Pilot and Test Condition

Pilot	Condition	Comfort Index 2				Comfort Index 3			
		Horizontal Disparity (minutes)		Vertical Disparity (minutes)		Horizontal Disparity (minutes)		Vertical Disparity (minutes)	
		Near	Far	Rt. Eye Low	Rt. Eye High	Near	Far	Rt. Eye Low	Rt. Eye High
A1	1A	↑	3.39	3.00	6.74	↑	2.22	2.50	5.50
	2A	12.00	3.00	2.40	5.26	↑	3.83	3.24	6.00
	3A	16.44	4.39	3.68	5.05	↑	4.04	3.56	4.60
	4A	↑	4.11	3.74	5.11	↑	3.68	3 47	6.29
	5A	↑	3.23	2.76	4.80	↑	3.60	3.16	5.40
	8A	↑	6.36	4.47	7.38	↑	4.12	4.20	6.98
	15A	↑	3.68	4.10	6.19	↑	3.61	3.26	5.60
A2	1A	0.00	0.00	0.00	0.00	8.25	0.00	3.21	3.00
	2A	↓	↓	2.29	1.05	4.76	4.11	3.56	3.18
	3A	0.78	0.60	3.00	↓	6.00	2.14	1.38	3.93
	4A	3.69	1.76	↓	↓	8.60	3.00	3.00	3.55
	5A	↓	↓	0.69	0.69	4.38	1.50	1.12	1.12
	8A	↓	↓	↓	↓	4.80	0.00	↓	6.24
	15A	3.90	↓	0.69	3.50	5.14	4.95	3.62	4.44
A3	1A	28.60	14.14	9.23	14.87	28.44	13.79	12.42	13.71
	2A	34.80	15.18	9.16	14.00	33.60	14.40	8.40	13.20
	3A	24.90	11.26	9.21	13.24	26.23	13.11	10.44	13.43
	4A	35.16	12.81	12.55	14.74	↑	13.42	13.12	15.24
	5A	↑	15.00	13.00	15.33	↑	16.80	12.46	15.43
	8A	↑	16.50	12.67	15.24	↑	18.55	13.71	18.23
	15A	28.00	12.00	8.08	12.00	26.00	13.50	9.60	12.46
N1	1A	5.54	18.54	1.70	2.17	20.35	19.29	6.43	11.05
	2A	↓	18.54	3.00	5.14	18.00	18.40	4.76	10.36
	3A	1.17	14.54	1.20	10.00	15.00	16.50	6.12	11.00
	4A	2.25	18.73	4.29	9.75	14.29	13.80	6.00	10.20
	5A	3.91	16.50	↓	10.25	18.95	18.43	7.04	↑
	8A	3.00	14.54	↓	5.05	22.86	21.90	6.91	12.22
	15A	4.14	14.85	0.00	10.50	22.80	15.26	6.47	10.41
N2	1A	↓	↓	0.45	3.00	8.57	↓	1.38	1.80
	2A	16.80	↓	0.00	0.00	↑	↓	1.76	1.76
	3A	↓	↓	↓	3.30	↑	↓	0.00	3.00
	4A	3.00	↓	↓	↓	12.00	0.00	↓	3.00
	5A	3.53	0.00	0.00	0.00	1.95	2.29	2.29	3.00
	8A	↓	↓	0.00	0.00	←	↓	↓	↓
	15A	7.06	↓	0.81	3.75	4.80	0.90	0.33	3.42
N3	1A	7.20	6.00	1.73	6.74	8.60	4.29	3.30	6.68
	2A	14.40	3.00	1.50	7.80	14.40	3.75	2.25	7.50
	3A	6.00	4.20	1.57	7.30	12.00	3.39	2.40	7.20
	4A	10.70	3.45	1.05	6.00	13.28	3.00	1.62	6.81
	5A	9.47	3.53	2.40	7.47	13.36	3.69	3.68	8.40
	8A	4.11	4.38	1.85	7.12	4.95	6.00	1.95	6.96
	15A	9.63	3.78	2.00	7.60	13.92	3.75	1.95	8.22

Table 7
Binocular Disparity Tolerances for Combined Conditions and for Populations of Pilots

Pilot	Condition	Comfort Index 2				Comfort Index 3			
		Horizontal Disparity (minutes)		Vertical Disparity (minutes)		Horizontal Disparity (minutes)		Vertical Disparity (minutes)	
		Near	Far	Rt. Eye Low	Rt. Eye High	Near	Far	Rt. Eye Low	Rt. Eye High
A1	1A,2A,15A	↑	3.43	3.26	6.07	↑	3.35	3.14	5.61
A2	↓	↓	1.00	1.25	5.54	4.09	3.51	3.54	
A3	30.32	14.12	8.08	14.03	28.80	13.87	10.07	13.17	
N1	2.83	16.87	2.25	9.15	20.68	18.29	6.12	10.50	
N2	↓	↓	0.46	3.16	↑	↓	0.95	2.25	
N3	10.29	4.20	1.79	7.29	12.75	3.75	2.57	7.33	
A1,A2,A3	14.40	3.33	3.00	6.13	11.54	3.95	3.50	5.29	
N1,N2,N3	6.68	1.70	1.40	5.29	14.00	1.74	3.00	5.00	
ALL	7.29	2.50	2.13	5.68	12.37	2.79	3.24	5.20	
A1	4A,5A	↑	3.72	3.32	4.97	↑	3.62	3.30	6.05
A2	0.69	0.41	0.00	0.00	7.06	1.64	1.85	2.40	
A3	↑	13.64	12.64	14.97	↑	13.89	12.96	15.33	
N1	3.13	18.00	3.67	9.94	16.04	16.04	6.48	10.80	
N2	3.20	↓	↓	↓	2.25	1.0[illegible]	1.12	3.00	
N3	10.04	3.50	1.81	6.69	13.33	3.20	2.45	7.15	
A1,A2,A3	14.40	2.59	2.73	5.37	13.60	3.50	3.19	5.25	
N1,N2,N3	6.75	1.50	1.00	5.21	13.50	2.25	3.18	5.40	
ALL	7.12	2.11	2.08	5.25	13.68	2.80	3.19	5.36	
A1	1A,4A,5A	↑	3.63	3.20	5.45	↑	3.33	3.16	5.00
A2	0.55	0.32	0.00	0.00	7.41	1.09	2.10	2.33	
A3	33.60	13.77	11.59	14.90	34.00	13.80	12.79	14.45	
N1	3.60	18.21	3.00	9.65	17.10	18.00	6.43	10.89	
N2	3.00	↓	↓	↓	0.00	0.00	1.20	2.00	
N3	9.41	4.33	1.79	6.72	12.16	3.50	3.00	7.00	
A1,A2,A3	14.70	2.61	2.58	6.13	13.71	2.79	3.10	5.70	
N1,N2,N3	6.68	1.80	1.14	5.25	12.00	1.86	3.26	5.36	
ALL	7.33	2.25	2.07	5.80	13.36	2.17	3.19	5.50	
A1	1A,2A,3A, 4A,5A,15A	↑	3.77	3.37	5.41	↑	3.58	3.27	5.57
A2	0.00	0.00	0.43	0.43	6.00	3.00	3.11	3.39	
A3	31.83	13.53	10.22	14.31	30.00	13.74	11.37	13.69	
N1	2.75	16.87	2.18	9.69	18.00	17.10	6.23	10.65	
N2	↓	↓	↓	↓	↑	↓	0.71	2.40	
N3	9.50	3.96	1.75	7.08	12.67	3.54	2.50	7.24	
A1,A2,A3	14.12	2.89	3.00	5.67	12.43	3.79	3.39	5.12	
N1,N2,N3	6.58	1.64	1.22	5.37	13.12	1.89	3.00	5.36	
ALL	7.21	2.40	2.10	5.53	12.60	2.79	3.17	5.20	

Table 7 Continues

Table 7 (Continued)
Binocular Disparity Tolerances for Combined Conditions and for Populations of Pilots

Pilot	Condition	Comfort Index 2				Comfort Index 3			
		Horizontal Disparity (minutes)		Vertical Disparity (minutes)		Horizontal Disparity (minutes)		Vertical Disparity (minutes)	
		Near	Far	Rt. Eye Low	Rt. Eye High	Near	Far	Rt. Eye Low	Rt. Eye High
A1	ALL	↑	3.92	3.54	5.67	↑	3.59	3.38	5.85
A2	↓	↓	0.00	0.00	6.00	2.62	3.00	3.24	
A3	32.18	14.03	10.62	14.46	30.97	14.00	12.08	13.93	
N1	2.75	16.50	1.67	9.58	18.40	18.00	6.29	10.82	
N2	↓	↓	↓	↓	↑	↓	0.43	1.20	
N3	9.20	4.04	1.76	7.10	12.27	3.69	2.50	7.21	
A1,A2,A3	14.47	3.75	3.23	6.07	12.69	3.94	3.44	5.54	
N1,N2,N3	6.22	1.50	1.20	5.21	12.43	1.83	2.77	5.31	
ALL	↓	7.17	2.37	2.14	5.65	12.63	2.79	3.18	5.36
A1,A2,A3	1A	15.51	2.59	2.34	6.71	14.22	1.77	3.00	6.16
↓	2A	9.90	2.44	2.46	4.50	8.18	4.32	3.57	4.38
	3A	13.17	3.60	3.86	4.94	16.87	4.00	3.37	4.87
	4A	15.19	6.00	4.50	6.30	13.93	4.06	3.68	6.11
	5A	13.00	1.69	2.18	4.09	13.31	3.00	2.37	3.75
	8A	16.41	7.14	6.46	7.26	14.57	6.39	4.00	7.08
	15A	16.57	4.10	4.12	6.00	12.26	4.17	3.67	5.68
N1,N2,N3	1A	6.00	2.46	1.39	5.00	11.00	1.09	3.43	5.10
↓	2A	6.45	0.43	0.75	4.67	16.00	1.67	3.07	4.14
	3A	5.00	1.91	1.05	6.20	12.00	1.31	1.89	6.00
	4A	6.80	0.75	0.67	4.76	13.25	1.70	2.20	4.89
	5A	6.75	2.06	1.41	6.25	13.76	3.00	4.04	6.25
	8A	0.60	0.19	0.40	4.20	3.90	2.00	2.33	4.80
	15A	7.07	1.96	1.71	5.69	16.00	2.62	1.89	6.12
ALL	1A	8.06	2.50	1.89	6.39	12.75	1.50	3.20	6.00
↓	2A	6.68	1.62	1.86	4.62	11.50	3.19	3.31	4.30
	3A	7.24	2.86	2.00	5.63	11.73	2.77	2.60	5.17
	4A	7.27	2.35	2.32	5.48	13.62	2.60	3.08	5.44
	5A	6.86	1.88	2.00	4.87	13.57	3.00	3.41	5.25
	8A	6.66	2.44	2.50	6.39	12.75	3.00	3.19	6.41
	15A	7.28	3.27	2.59	5.79	13.76	3.55	3.16	6.00

seven matched samples, representing the data for the seven conditions using the same six test subjects, could have been drawn from the same population, i.e., the null hypothesis that there are no differences among test conditions. A sample analysis is presented in Table 8. The binocular disparity tolerances for the seven test conditions are ranked for each of the pilots, and the sum of the ranks is determined for each test condition. The statistic

$$X_r^2 = \frac{12}{Nk(k+1)} \sum_{j=1}^{k} (R_j)^2 - 3N(k+1),$$

Table 8
Friedman Two-Way Analysis of Variance
Among Test Conditions

Vertical Disparity—Comfort Index 3							
Condition	Disparity Tolerance (minutes of arc)						
	1A	2A	3A	4A	5A	8A	15A
Pilot							
A1	2.50	3.24	3.56	3.47	3.16	4.20	3.26
A2	3.00	3.18	1.38	3.00	1.12	↓	3.62
A3	12.42	8.40	10.44	13.12	12.46	13.71	9.60
N1	6.43	4.76	6.12	6.00	7.04	6.91	6.47
N2	1.38	1.76	0.00	↓	2.29	↓	0.33
N3	3.30	2.25	2.40	1.62	3.68	1.95	1.95
Ranked Data—Among Conditions							
Pilot							
A1	1	3	6	5	2	7	4
A2	4.5	6	3	4.5	2	1	7
A3	4	1	3	6	5	7	2
N1	4	1	3	2	7	6	5
N2	5	6	3	1.5	7	1.5	4
N3	6	4	5	1	7	2.5	2.5
R_j	24.5	21	23	20	30	25	24.5

$$X_r^2 = \frac{12}{Nk(k+1)} \sum_{j=1}^{k} (R_j)^2 - 3N(k+1) \qquad \begin{matrix} N=6 \\ k=7 \end{matrix}$$

$$X_r^2 = 2.27 \qquad P = 0.89$$

where

N = number of rows (pilots)

k = number of columns (conditions)

R_j = sum of ranks in jth column

is then computed. This statistic is distributed as X^2 with $(k - 1)$ degrees of freedom. The value of X^2 obtained in Table 8 is 2.27, and the probability of obtaining a value equal to or larger than this figure is 0.89. Hence, it is quite likely that the data for all seven test conditions could have been drawn from the same population, and there is no basis for claiming differences among the test conditions.

Analyses similar to Table 8 were performed for vertical disparity tolerances under Comfort Indices 2 and 3, using the lower of the hypophoric and hyperphoric values, and for each of these vertical phorias individually, and for esophoric and exophoric horizontal disparities. The results are summarized in Table 9. In no instances is the probability lower than that which may reasonably be expected by chance. The minimum probability level is 0.30. Therefore, there is no statistical basis for inferring differences in disparity tolerances among the various test conditions for the sample of six pilots used in this study.

Table 9
Summary of Friedman Two-Way Analyses of
Variance for Binocular Disparity Tolerances
Among Test Conditions

Type of Disparity	Comfort Index	Probability $\chi^2 > \chi_r^2$
Vertical—Rt. Eye Low	2	0.54
Vertical—Rt. Eye High	2	0.36
Vertical—Min. Value	2	0.40
Vertical—Rt. Eye Low	3	0.77
Vertical—Rt. Eye High	3	0.59
Vertical—Min. Value	3	0.89
Horizontal—Convergent	2	0.30
Horizontal—Divergent	2	0.84
Horizontal—Convergent	3	0.99
Horizontal—Divergent	3	0.47

These results are due to the larger differences among the pilots than among the test conditions (Tables 6 and 7).

Differences among the pilots were investigated further for the data in Table 8 by using the same type of analysis of variance among the pilots, considering the data for the pilots as six matched samples. The results are shown in Table 10. The X_r^2 value of 30, with 5 degrees of freedom, is highly significant at a probability less than 0.001. Hence, the differences among the pilots preclude any inferences that they could have been drawn from a common population with respect to visual tolerances to binocular disparities.

The preceding analysis of variance among test conditions considered all seven test conditions simultaneously. It is interesting to compare sets of two conditions, and the Sign Test (5) has been selected for this purpose. This is a nonparametric analysis of the differences between the binocular disparity tolerances for the two conditions being evaluated for each of the six test subjects. If there were no differences between conditions, the expected number of positive and negative signs for these differences would be expected to be approximately equal among the six pilots. Vertical disparity tolerances under Comfort Index 3 were selected for this analysis, which is presented in Table 11 for Conditions 1A and 2A. The result is a probability of 0.656, which is quite likely to occur by chance. Hence, no differences between these two conditions can be inferred. The results of similar analyses for all 21 combinations of the seven test conditions taken two at a time are presented in Table 12. None of these differences can be considered statistically significant, using a probability level of 0.05 as the criterion.

The binocular disparity tolerances for each of the pilots and test conditions, as well as combinations of conditions and pilots, are summarized in Tables 6 through 7. These data may more easily be assimilated and compared if presented in a graphic form, and the scheme shown in Figs. 8 through 16 was evolved for this purpose. In preparing these charts, the data in the tables were first converted from minutes of arc to milliradians (3.44 minutes = 1 mrad). Disparities up to 3.0 mrad are shown in the figures, with an arrowhead

Table 10
Friedman Two-Way Analysis of Variance
Among Pilots

Vertical Disparity—Comfort Index 3								
Condition	Ranked Data—Among Pilots							
	1A	2A	3A	4A	5A	8A	15A	R_j
Pilot ↓								
A1	2	4	4	4	3	4	3	24
A2	3	3	2	3	1	1.5	4	17.5
A3	6	6	6	6	6	6	6	42
N1	5	5	5	5	5	5	5	35
N2	1	1	1	1	2	1.5	1	8.5
N3	4	2	3	2	4	3	2	20

$$\chi_r^2 = \frac{12}{Nk(k+1)} \sum_{j=1}^{k} (R_j)^2 - 3N(k+1) \qquad \begin{matrix} N=7 \\ k=6 \end{matrix}$$

$$\chi_r^2 = 30 \qquad P < 0.001$$

Table 11
Sign Test for Comparison of
Test Conditions 1A and 2A

Vertical Disparity—Comfort Index 3

Condition	Minutes of Arc		Sign
	1A	2A	(1A-2A)
Pilot ↓			
A1	2.50	3.24	−
A2	3.00	3.18	−
A3	12.42	8.40	+
N1	6.43	4.76	+
N2	1.38	1.76	−
N3	3.30	2.25	+

For N=6 & X =3, P=0.656
From Table D, Reference 5

Table 12
Summary of Sign Tests for Comparison of
Test Conditions in Pairs

Condition	Probability of Obtaining						
	1A	2A	3A	4A	5A	8A	15A
1A	—	0.656	0.109	0.500	0.109	0.656	0.656
2A		—	0.344	0.344	0.344	0.656	0.344
3A			--	0.344	0.344	0.656	0.656
4A				—	0.656	0.188	0.344
5A					—	0.344	0.344
8A						—	0.500
15A							—

indicating values larger than 3.0 mrad. Vertical disparity tolerances are presented on the vertical axis, with upper segment representing right eye high and the lower segment indicating right eye low. Convergent (near) tolerances are shown to the left on the horizontal axis, and divergent (far) values are plotted to the right.

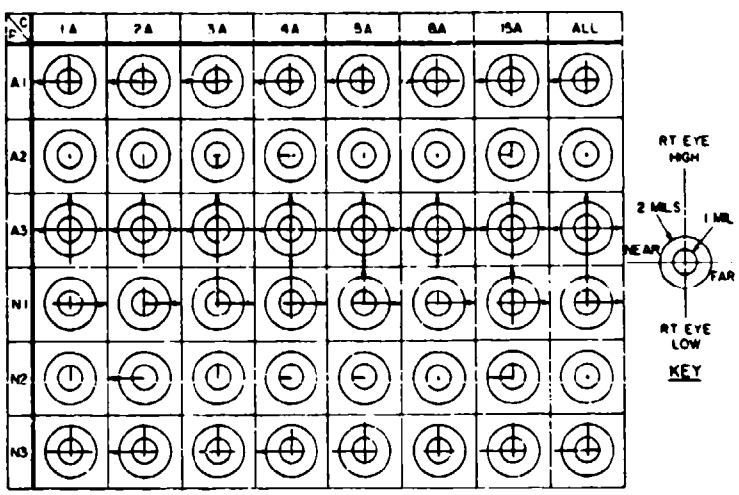

Fig. 8—Summary of binocular disparity tolerances for Comfort Index 2

The mapped tolerances for each of the pilots under each of the conditions are shown in Figs. 8 and 9 for Comfort Indices 2 and 3. Plots for the lower of the values from the two indices are presented in Fig. 10. Figures 11 through 16 show plots for individual and combined conditions for the Army pilots combined, the Navy pilots combined, and all pilots combined. The individual conditions with pilots pooled are shown in Figs. 11 through 13, for the two comfort indices, and the minimal values. Comparable data for combinations of conditions are shown in Figs. 14 through 16.

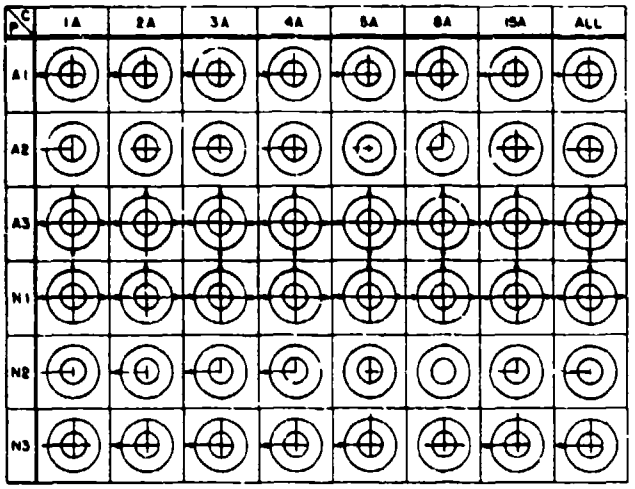

Fig. 9—Summary of binocular disparity tolerances for Comfort Index 3

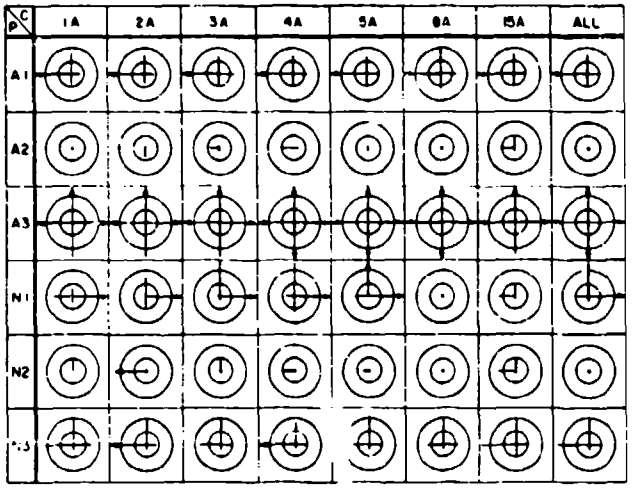

Fig. 10—Summary of minimal bincoular disparity tolerances

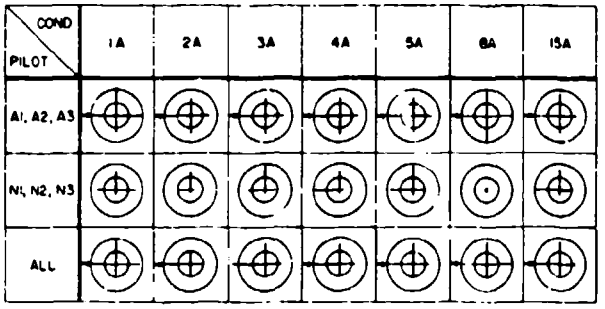

Fig. 11—Summary of binocular disparity tolerances for populations of pilots—Comfort Index 2

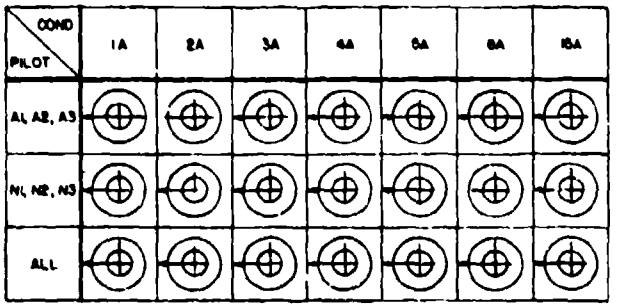

Fig. 12—Summary of binocular disparity tolerances for populations of pilots—Comfort Index 3

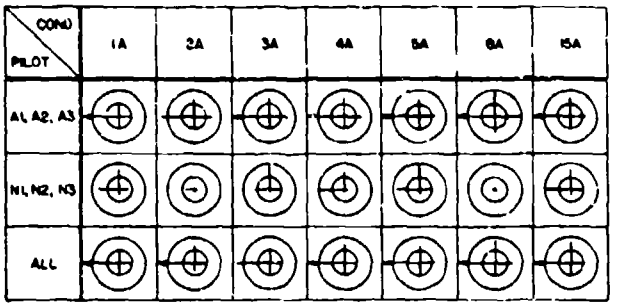

Fig. 13—Summary of minimal binocular disparity tolerances for populations of pilots

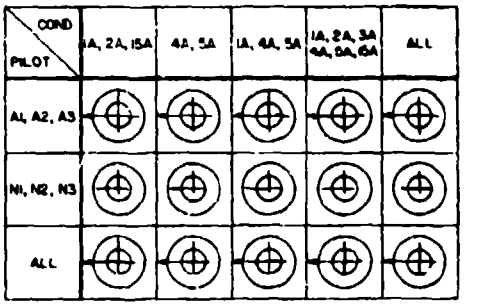

Fig. 14—Summary of binocular disparity tolerances for populations of pilots with combined conditions—Comfort Index 2

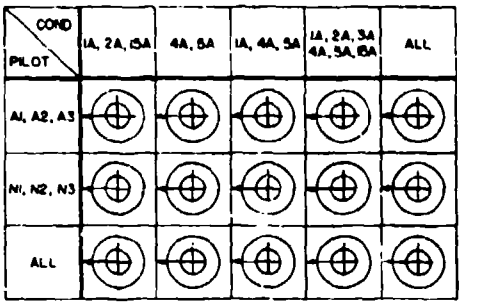

Fig. 15—Summary for binocular disparity tolerances for populations of pilots with combined conditions—Comfort Index 3

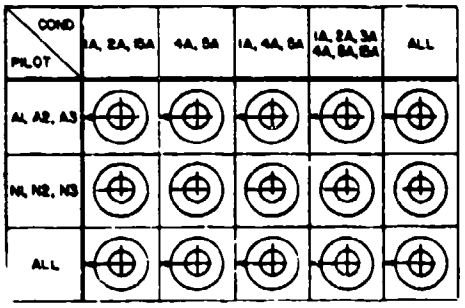

Fig. 16—Summary of minimal binocular disparity tolerances for populations of pilots with combined conditions

Results and Implications

The charts which summarize the binocular disparity tolerances for each of the six pilots under each of the seven test conditions are shown in Figs. 8, 9, and 10 for Comfort Indices 2 and 3. While the differences among test conditions are small for each pilot, the differences among the pilots is striking. This would indicate that the pilots have their visual idiosyncrasies in responding to binocular disparities. It is instructive to correlate the test results with the data obtained in clinical optometric examinations of the pilots. The examinations were performed by the registered Optometrist on the Sperry Medical Staff (Herman Sager, O.D.), and the results are shown in Table 1. Dr. Sager was also the optometric consultant in this study.

Ranges of values for subjects with what is clinically considered normal vision are also included in this table. The optometric data were obtained for four subjects only. The first two subjects, A1 and A2, were no longer available for examination when the significant differences among the assigned test subjects were recognized. The data obtained with three subjects in Phase 1 of this study were much more consistent (1).

The phorias in Table 1 are the relative directions of the two eyes in the absence of an adequate fusion stimulus. They are expressed as angles in prism dioptus; a prism diopter is an angle whose tangent is 0.01. Exophoria indicates divergence of the eyes, while esophoria indicates convergence. The ductions are the movements of the eyes in opposite directions to maintain fusion of a stimulus at a given distance. The break point is the angle between the eyes at which diplopia, or double vision, occurs when this angle is gradually increased. The recovery point is the angle at which fusion is regained as the angle is gradually decreased from the value at which diplopia occurred. The duction data in Table 1 indicate that there is always a hysteresis effect in the cycle from single to double vision and back again to single vision, i.e., recovery occurs at a somewhat lower angle than that which produced diplopia. The ductions in Table 1 cover the two horizontal directions (induction and outduction), and the two vertical directions (suproduction, or right eye high, and subduction, right eye low). The refractive errors are expressed as prescriptions for spherical corrections for myopia (−) and hyperopia (+), and cylindrical corrections for astigmatism, if present.

Since no significant differences exist among test conditions, the tolerances obtained by merging all data shown in the columns on the extreme right in the tables can be used for evaluation. Furthermore, the minimal levels obtained from both comfort indices (Fig. 10) can be used as criteria, as in Phase I. The tolerances of pilot A3 for binocular disparities exceed 3 mrad in both directions in the horizontal and vertical axes. His phorias are within the normal range (Table 1), and his ductions are just below this range. Note that this subject had two examinations, 7 days apart, with marked increases in the measured ductions. This is due to the dependence of the ductions on the eye muscles; therefore, the ductions are subject to training. The continuing exposure to binocular disparities during the tests probably contributed to this improvement, and there may have been further improvement after the second examination. Clearly, from Fig. 10, subject A3 had the largest tolerances to binocular disparities of all six subjects.

In comparing binocular disparity tolerances, shown in the data charts in Fig. 10 in milliradians, and the phorias and ductions in Table 1, expressed in prism diopters, it should be appreciated that a milliradian is one-tenth the magnitude of a prism diopter. The break points obtained in the Maddox rod duction tests are the binocular disparities of stimuli, viewed against a homogeneous dark background, which are sufficient to cause image doubling. These may be expected to be considerably higher than the computed disparity tolerances for two reasons. Tolerances are much higher for disparities viewed against a homogeneous background as compared with an articulated background such as the real world. This was demonstrated in Phase I (1), where the ratio between these tolerances exceeded a factor of 10. Also, the criteria used in determining tolerances involve visual comfort (Comfort Indices 2 and 3), and not the extreme situations involving image doubling, which correspond to comfort levels 5 and 6 in the response repertory of the test subjects.

The esophoric lateral tolerance of pilot N1 and one of his vertical tolerances were both less than 1 mrad (Fig. 10). Examining his clinical data in Table 1, a lateral exophoria of 1 prism diopter is shown. His induction is also low, so that he could not easily compensate for this exophoria. Consequently, the low tolerance to esophoric disparities is consonant with the clinical data. The vertical recovery point of his vertical tolerances is one prism diopter in both directions, which would tend to make him susceptible to fatigue when subjected to vertical disparities, which can account for his low tolerance.

The tolerances of pilot N2 were low in all directions (Fig. 10). His optometric data indicate 4-5 prism diopters of esophoria, with low outductions. His ductions in the vertical direction are also low (Table 1). These data were consistent for two examinations and explain his low tolerances. From Fig. 10, it is seen that pilots A2 and N2 had comparably low tolerances. Clinical data are not available for pilot A2. He was the first subject manifesting these extreme results. After he had completed his test regimen, however, he was asked to rate the visual comfort of sharp, high contrast printed paper copy, and he indicated a comfort level of only 2, i.e., comfortable, short of excellent. This would seem to imply the presence of some clinical questions.

Pilot N3 has binocular disparity tolerances (Fig. 10) which are consistent with other data commonly obtained in these studies, and his clinical data in Table 1 are normal in all respects.

The correlation between the pilots' tolerances for binocular disparities in head-up displays and the Maddox Rod test results for phorias and ductions has implications for predicting pilots' visual comfort with displays which generate such disparities. It is important

to recognize that only those head-up displays which have exit pupil configurations which permit binocular viewing of the imagery can produce these disparities. Under these conditions, the Maddox Rod test, which can readily be administered by a qualified optometrist, may be used as a qualitative indicator of a pilot's visual comfort under a given set of disparities.

On the basis of the data in Fig. 10, disregarding the results for subjects A2 and N2 due to their clinical correlates, as well as the esophoric tolerance of pilot N1 for the same reason, some conclusions regarding permissible binocular disparity tolerances may be drawn. Horizontal tolerances of 1-mrad exophoria (divergence) and 2.5-mrad esophoria (convergence) are reasonable. In the vertical axis, a tolerance of 1 mrad in both hyperphoric and hypophoric ductions is also indicated. These figures are also consonant with the results obtained by combining the raw data for both the subject populations, though limited, and the test conditions (Fig. 16).

The recommended tolerances obtained in this study are the same as those from Phase I. The difference between the two studies is the dynamic real world background used in the present program, compared with a static real world in Phase I. Therefore, it may be concluded that the presence of a dynamic real world background in lieu of a static real world does not significantly affect the permissible binocular disparities when viewing moving images in head-up displays.

STEREOPSIS IN VISUAL FLIGHT

General

Pilots control their aircraft in three dimensions, usually under visual conditions, and spatial localization is therefore a critical operation in many flight maneuvers. These maneuvers include approach and landing, hovering of helicopters and VTOL aircraft, terrain following, formation flying, and collision avoidance. In fact, the effectiveness and safety of all flight operations in which there is proximity to the ground or other aircraft presently rely heavily on visual space perception by the pilot.

Distance judgement or depth perception is an important aspect of space perception. In this regard, it is important to distinguish between absolute distance and relative depth. In the perception of absolute distance, the actual distances of objects in space from the observer are visually experienced and estimated, in what may be psychologically termed egocentric localization. Relative depth represents the extent to which one object appears nearer to or farther from an observer than a second.

The visual cues for the judgement of distance can be monocular or binocular. Monocular cues are of course always present in binocular vision and must therefore be considered in any analytical or experimental evaluation of the effectiveness of binocular cues. The principal monocular cues to distance are

- Size, wherein distances are estimated by the angular subtenses of objects of known size or relative subtenses of objects of the same size,
- Overlay, or interposition, in which objects nearer the observer visually occlude parts of more distant objects lying in the same visual direction,

- Linear perspective, the visual convergence of parallel lines which recede in the distance, e.g., the longitudinal edges of a runway;
- Aerial perspective, in which objects seen at a distance have less distinct contours, and differences in color, saturation, brightness, and contrast than proximal objects, all due to the photometric effects of the intervening atmosphere;
- Light areas and shadows, which help define the position and angular orientation of objects in relation to the existing sources of illumination;
- Motion parallax, changes in the relative angular positions of objects as the body and/or the head of the observer move;
- Accommodation, muscle sensory cue as a result of focusing changes in the eye to maintain a sharp image on the retina.

There are two binocular cues, stereopsis and convergence. Stereopsis, with which this study is principally concerned, involves the differences in the monocularly generated images in the two eyes due to the difference in the positions of the eyes in space, i.e., the interpupillary separation. Convergence is the muscle sensory cue caused by the convergence of the eyes required to fixate on an object which is not at visual infinity in space. Although stereopsis presupposes fixation on some object, convergence and stereopsis are not related. The myosensory cues (accommodation and convergence) are weak relative to the other cues generally available for the perception of distance.

Some of the basic geometry related to stereopsis is shown in Fig. 17. Point F, in the median plane, is fixated by an observer, so that the images f_L and f_R are on the foveae of the left and right eyes. A second point A, displaced from F in the longitudinal direction by ΔX and the lateral direction by Δy, so that the displacement vector FA is given by $(\Delta X + j\Delta y)$, is also seen by the observer. The lateral direction is given the j designation. If the displacement of A were in the longitudinal direction only, i.e., to point A_X, the images of A_X would be at a_{XL} and a_{XR} on the two retinas. These are not corresponding points on the retinas, since the angle α_{XL} is generated by a counterclockwise sweep from $O_L F$ to $O_L A$, while the angle α_{XL} is formed by a clockwise sweep from $O_R F$ to $O_R A_X$. The algebraic difference between the two angles α_{XL} and α_{XR} (one is positive and the other is negative) is the magnitude of binocular disparity. A longitudinal separation between two objects will therefore produce a binocular disparity.

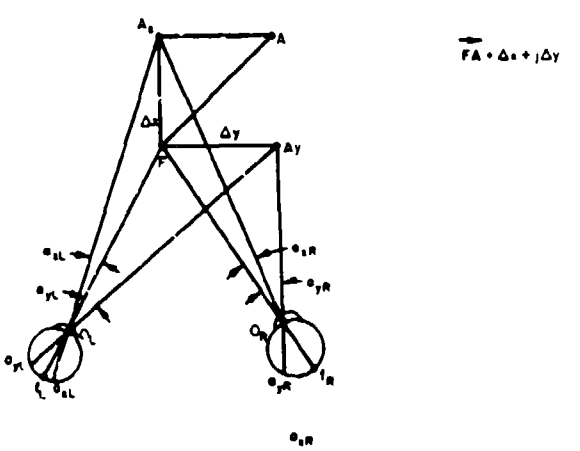

Fig. 17—Stereopsis related to differences in spatial positions of objects

Now consider a displacement in the lateral direction only to point A_y. The images of A_y will be at a_{yL} and a_{yR}, and, for small values of Δy relative to the longitudinal distance from the observer to point F, the angles α_{yL} and α_{yR} will be equal and of the same algebraic sign. The binocular disparity, which is the difference between α_{yL} and α_{yR}, will be zero, and points a_{yL} and a_{yR} are on corresponding points of the two retinas. Therefore, a lateral separation between two points will not produce a binocular disparity. When small visual angles are involved, as in the preceding discussion, and the displacement between two points has both longitudinal and lateral components, only the longitudinal component produces the binocular disparity, and hence the stereopsis.

The geometric relationships become somewhat more complex when large visual angles between two points in space are involved. Under these conditions, horopters must be considered. The horopter is a surface defining the locus of object points in space which simultaneously stimulate corresponding points on the retinas under given conditions of binocular fixation (6-8). The simplest form of horopter for vision in a single plane is a circle passing through the centers of rotation of the two eyes (O_L and O_R) and the fixation point F, as shown in Fig. 18. This circle is the locus of point A for which the angles α_1 and α_2 are equal, so that the inscribed angles γ_1 and γ_2 must also be equal. The horopter in this case is called the Vieth-Muller circle, named after its promulgators. For the task of evaluating stereopsis in visual flight, the horopters in a given plane may be considered straight lines parallel to the interocular axis $O_L O_R$, i.e., circles of infinite radius, since the visual angles involved are small. The depth differences between the fixation and a second point on the circular horopter (Fig. 18) as a fraction of the distance to the fixation point is given by α^2, where α is the visual angle between the two points, in radians. For an angle of 0.01 rad (0.57 degree), this relative depth difference is only 0.01 percent, while at a peripheral angle of 0.1 rad (5.73 degrees), the difference is still only 1.0 percent.

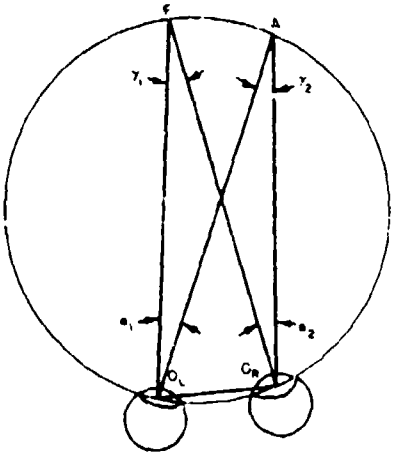

Fig. 18—Vieth-Muller circle illustrated as a horopter in the horizontal plane

When the disparate point A_X is placed beyond the fixation point F (Fig. 17) sufficiently to produce two images of A, and the right eye is closed, the right-half image a_{XR} will disappear. The same will happen for the left eye and the left-half image a_{XL}. The images a_{XL} and a_{XR} are considered to be *uncrossed* disparate. If, however, point A_X were closer to the observer than the fixation point, closing the right eye would cause the left-half image to disappear, and conversely for the left eye. The two images of A_X would be *crossed* disparate under these conditions. The terms crossed and uncrossed are frequently used to denote disparities produced by objects closer to and farther from the fixation point, when both objects lie in the median plane. This terminology will however be avoided in this report in favor of the simpler terms *near* and *far*, which describe real stimulus situations more clearly.

Stereopsis is the principal binocular phenomenon which gives rise to visual localization in space. However, there are additional binocular cues used in space perception which are empirical, i.e., learned through experience, and which may supplement stereopsis or may provide independent clues. These generally relate to differences between the two retinal images at near vision. They may be classified into four types of cues:

- Binocular differences in perspective and visibility, e.g., a cube viewed orthogonally by one eye, so that only one face is seen, while the other eye can see two faces. Differences in the perceived shapes of all faces seen by the eyes represent a more general situation of this type.

- Binocular parallax, e.g., objects which are in front of a background to which they may be related, such as a grid. There will be differences in the grid positions which are seen as overlayed by each of the eyes, due to the difference in eye positions.

- Binocular differences in image size due to location, e.g., an object displaced from the median plane and seen with near vision will have retinal images of different size, due to the different distances from the eyes and their effect on visual magnification.

- Binocular differences in image gradient with known patterns in objects. This is more subtle phenomenon involving rates of change in disparities and shapes with distance (gradients) for the images in the two eyes for certain object patterns. The gradients are larger at the shorter distances and hence provide the observer with clues to distance. These are differential gradients and are not the same as textural gradients associated with monocular perception of patterns in depth (9).

A comprehensive treatment of binocular phenomena is contained in Ref. 6. Precision of depth localization with stereopsis involving double images is presented in Ref. 10. Limits of stereopsis for central and peripheral vision up to 6 degrees of arc have been investigated in Ref. 11, and a recent survey of some current theoretical issues is included in Ref. 12.

Relationships in Stereopsis

The quantitative relationships among the factors involved in stereopsis are developed in Appendix A. The binocular disparity θ_d between two points which are in different positions in the visual field is given by

$$\theta_d = \frac{p\Delta r}{r(r + \Delta r)}, \tag{1}$$

where p is the interpupillary distance, r is the distance from the observer to the near point, measured normal to the interocular axis, and Δr is the normal distance between the two points. The magnitude of the disparity is independent of which of the two points is fixated. If the near point is considered to be the fixation point, the convergence angle for fixation is $\theta_f = p/r$. If the dimensionless depth ratio $\Delta r/(r + \Delta r)$ is designated as σ_r, the disparity may be expressed simply as

$$\theta_d = \theta_f \sigma_r. \tag{2}$$

Another convenient form for Eq. (1) is

$$\theta_d = pK_r, \tag{3}$$

where the parameter K_r is $\Delta r/r(r + \Delta r)$, and therefore has the dimension 1/distance. K_r is also a useful parameter for evaluating motion parallax, to be discussed in this section.

For any given near point, the maximum disparity occurs when the far point is at visual infinity, and its magnitude is equal to the convergence angle θ_f.

Another useful relationship involves the parallax angles subtended by the two points for the left and right eyes, α_L and α_R. The binocular disparity is the algebraic difference between these angles:

$$\theta_d = \alpha_L - \alpha_R \tag{4}$$

Motion Parallax and Related Phenomena

Motion parallax, which is a monocular cue to distance judgment, is the rate of change in the relative angular positions of objects in space as the observer's head is in motion, due to body motion, head motion, or both (7). The equations for evaluating motion parallax are developed in Appendix B. For lateral motion with a rate $\dot{y} \equiv dy/dt$, the motion parallax $\dot{\alpha}_y$ in radians per second is

$$\dot{\alpha}_y = \dot{y}\left[\frac{\Delta r}{r(r + \Delta r)}\right] = \dot{y}K_r \tag{5}$$

and

$$\dot{\alpha}y/\alpha = \dot{y}/y. \tag{6}$$

Equation (6) indicates that the relative rate of change of monocular parallax angle $\dot{\alpha}y/\alpha$ is equal to the relative rate of change of lateral displacement from the line joining the two points involved in the parallax. Also the rate of change in binocular disparity $\dot{\theta}_d$ is zero for lateral motion.

For longitudinal motion $\dot{r} = dr/dt$, the motion parallax $\dot{\alpha}_r$ is

$$\dot{\alpha}_r = -2\alpha\frac{\dot{r}}{r_h} \text{ or } \frac{\dot{\alpha}_r}{\alpha} = -2\frac{\dot{r}}{r_h}, \tag{7}$$

where r_h is the harmonic mean between the distances r and $r + \Delta r$, i.e.,

$$\frac{1}{r_h} = \frac{1}{2}\left[\frac{1}{r} + \frac{1}{(r + \Delta r)}\right].$$

The negative sign in Eq. (7) indicates that $\dot{\alpha}_r$ will be positive (increasing parallax angle) when r is negative, i.e., closing range. With longitudinal motion, the binocular disparity will be changing, and its rate is given by

$$\dot{\theta}_{dr} = -2\theta_d\frac{\dot{r}}{r_h} \text{ or } \frac{\dot{\theta}_{dr}}{\theta_d} = -2\frac{\dot{r}}{r_h}. \tag{8}$$

The relative binocular disparity rate $\dot{\theta}_{dr}/\theta_d$ and the relative rate of change of monocular parallax angle $\dot{\alpha}_r/\alpha$ are therefore equal for longitudinal motion of the observer.

When two points are separated laterally by a distance d, and the observer is located at a range r from these points (Fig. 19), the angular subtense of the points is given by $\epsilon = d/r$, for small angles ϵ. The distance d may be the width or extent of an object in space. The rate of change of the angle produced by the observer approaching the object at a rate $\dot{r}$ is therefore

$$\dot{\epsilon}_r = -\frac{d}{r^2}\dot{r} = -\epsilon\left(\frac{\dot{r}}{r}\right), \tag{9}$$

where the negative sign implies increasing ϵ for a closing range (negative $\dot{r}$). The ratio $r/(-\dot{r})$ is the time to impact T. Therefore, from Eq. (9),

$$\dot{\epsilon}_r/\epsilon = 1/T, \tag{10}$$

which indicates that the relative rate of increase in subtended angular size is the reciprocal of the time to impact in closing longitudinal motion. The visually perceived increasing ϵ is the "looming" phenomenon.

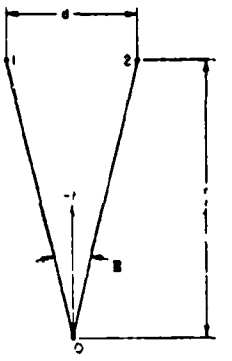

Fig. 19—Dynamics of changing angular subtense with radial velocity

Evaluation of Stereopsis in Depth Perception

The multiplicity of monocular cues for the perception of depth in the real world, augmented by several binocular cues including stereopsis, introduces subtleties into the task of evaluating the relative importance of stereopsis per se. It is essential to obtain data describing the capabilities of the human observer in depth perception using pure stereopsis, i.e., where the only clues to distance discrimination are binocular disparities between the two retinal images. Fortunately, Ogle (6) has developed an optical method for changing the angular disparity between the images of two lights in the two eyes which eliminates possible empirical cues which may affect the results. One such cue may be perceived brightness changes in the lights due to differences in the distances from the observer.

Binocular disparities were generated with different magnifications in the viewing systems for the two eyes, and the distances from the observer to the stimuli were maintained constant. The results for three test subjects are shown in Fig. 20. Stereoscopic thresholds are plotted as functions of the angular separation of the light sources. Separations as large as 14 degrees are involved, so that these data cover peripheral vision, as well as

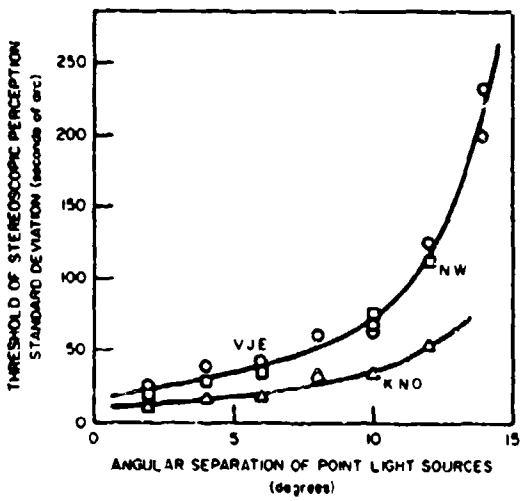

Fig. 20—Thresholds for stereopsis as a function of lateral angular separation between test points (6)

central vision at the lowest separation of 2 degrees. The threshold is expressed as a standard deviation of the disparity, taken from a psychometric curve (13) so that approximately 68 percent of the judgments are made within the stimulus boundaries established by plus and minus one standard deviation. Figure 20 indicates the accelerating rise in threshold, i.e., lower stereoscopic sensitivity, as the angular separation between stimuli is increased. For interpreting the angles, it should be noted that the tests were conducted with a fixation point in the median plane midway between the stimuli. The fixation point was extinguished when the stimuli were presented for a duration of 2 seconds. Hence, the disparate retinal stimulations in Fig. 20 occurred symmetrically at half the indicated angles from the center of the fovea. The minimal thresholds at low angles generally agree with comparable data obtained by other investigators (7). An indication of the variation in thresholds which can be expected as a result of individual differences may also be noted from Fig. 20.

A common numerical base is required to compare depth perception by means of stereopsis, with other cues available to an observer, for example, a helicopter pilot. The results of such comparisons should be expressed in terms of the distances over which the various cues are most effectual. All cues to depth perception diminish as a function of distance, but not at the same rates, nor do they have the same initial values at short distances. A useful base for expressing the effectiveness of a cue is the standard deviation of the distribution of the increments in distance required to detect a difference in location in depth between two objects or targets at a given range. Field experiments have been performed to measure such thresholds under both monocular and binocular conditions (14,15). These depth increments may be converted to equivalent binocular disparities expressed as angles, and vice versa, by means of Eq. (1). In this study, the distance increments have been selected as a standard, and thresholds associated with different cues (Δr) will be determined as a function of distance r. On this basis, a binocular disparity threshold θ_d is converted to a depth increment by the relationship

$$\Delta r_{\theta_d} = r^2 \left[\frac{p}{\theta_d} - r \right]^{-1} \tag{11}$$

from Eq. (1). Similarly, for motion parallax due to lateral motion of the observer $\dot{y}$, the depth threshold is given by

$$\Delta r_{\dot{y}} = r^2 \left[\frac{\dot{y}}{\alpha_t} - r \right]^{-1}, \tag{12}$$

where α_t is the threshold for motion parallax. Equation (12) is obtained from Eq. (5).

For longitudinal motion parallax ($\dot{r}$), the depth threshold is

$$\Delta r_{\dot{r}} = \left(\frac{\alpha_t}{\alpha_f r \dot{r}} + \frac{1}{r^2} \right)^{-1/2} - r, \tag{13}$$

where α_f is the lateral displacement angle from the observer to the fixation point. A plot of each of these functions of Δr in terms of the distance r on a common set of coordinates will provide an indication of the relative effectiveness of these three cues to depth perception at various ranges. The cue with the *lowest* threshold at a particular distance will be the most effective due at that range. Log-log coordinates have been selected as most suitable for these plots for several reasons. Large ranges of values for r and Δr were required, without deemphasizing relative changes in these variables at the lower values. Also, the functions are almost linear on log coordinates for the ranges of values covered. Finally, a vertical displacement of a value of Δr is a measure of a ratio of values, and hence relative, rather than an absolute, difference. Comparisons are therefore more graphic on logarithmic coordinates than on linear coordinates.

Some plots were made as described above and are shown in Fig. 21. Two binocular disparity curves are presented, one for a threshold of 10 seconds of arc representing an observer with a low threshold in foveal vision, and the second with a threshold of 70 seconds, for observers with higher threshold, at an angular separation of 10 degrees between test points (Fig. 20). These curves are slightly concave upward, and they have vertical asymptotes at value of range r equal to 628 feet for θ_d = 70 seconds, and 4400 feet for θ_d = 10 seconds. These values of r are the maximal distances for stereopsis at the thresholds being considered.

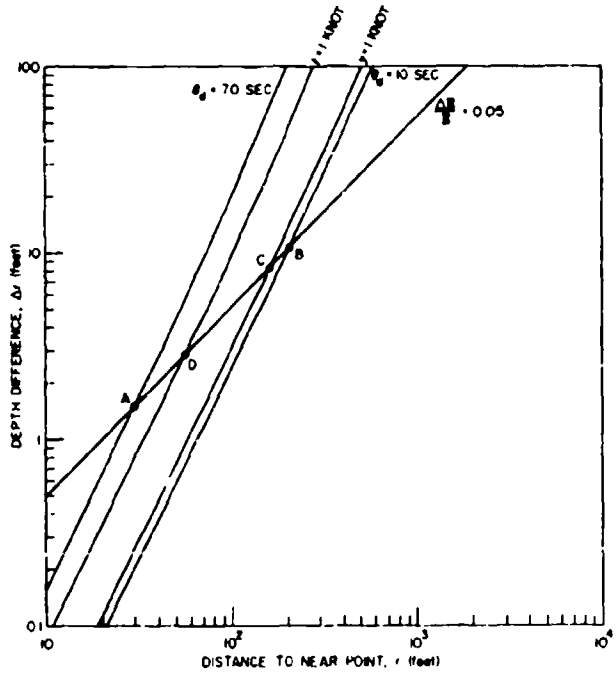

Fig. 21—Thresholds for perception of differences in depth as a function of distance for various perceptual processes

For lateral motion parallax, a lateral velocity $\dot{y}$ of 1 knot has been selected and a threshold for motion parallax $\dot{\alpha}_t$ of 100 seconds of arc per second (7). The resulting plot of Eq. (12) is shown in Fig. 21. Equation (13) has also been plotted in Fig. 21, for longitudinal motion parallax using a closing speed $\dot{r}$ of 1 knot, the same motion parallax threshold α_t of 100 seconds of arc per second, and a lateral displacement angle α_f of 10 degrees. The superiority of lateral motion to longitudinal motion is demonstrated in Fig. 21 by the lower placement of the $\dot{y}$ curve. Although the four curves described are sensibly parallel, they are curvilinear, concave upward. Therefore, the ratio between any two thresholds does not remain constant as distance increases, but actually rises. This may also be deduced from Eqs. (11) through (13).

There have been field studies in which targets such as rectangular boards and cylindrical tubes were used to determine monocular and binocular thresholds for depth perception (14,15); minimal distances were 200 feet, and the more comprehensive study (14) went to distances as high as 3000 feet. Some superiority is demonstrated for binocular viewing, but results are not consistent as functions of range and are subject to artifacts in the experimental situation. For example, the use of a sloping surface produces enhanced differential vertical separation between the tops of the targets as the targets are separated in range. This introduces vernier acuity considerations for threshold. Computed stereopsis angles in the binocular situation are very low, varying from 4 seconds of arc down to about 1 second, all at ranges below 1400 feet, which is within the range for stereoscopic vision. Ratios between binocular and monocular thresholds are not large (14). These studies, however, are suggestive to the use of a differential size threshold as the perception of difference in depth. As Gibson points out in Ref. 9, the perception of size is intimately related to the perception of distance. There are differences in the retinal sizes of two identical objects at difference distances, even if size constancy prevails. This retinal image difference is then perceptually recognized as a difference in depth. The systematic variation in retinal size of a textured surface with distance is the basis for the gradient of density of texture (9).

The use of differential retinal size as the determinant of a difference in distance leads to the relationship

$$\Delta r = (\Delta\epsilon/\epsilon)r, \tag{14}$$

where $\Delta\epsilon/\epsilon$ is the threshold for the perception of retinal size differences. A value of the standard deviation of the parameter $\Delta\epsilon/\epsilon$ of 0.05 has been established in Ref. 16. Equation (14) has been plotted in Fig. 21 using this value of $\Delta\epsilon/\epsilon$. It is a straight line with a slope of unity and a vertical orientation determined by the value of $\Delta\epsilon/\epsilon$. A low threshold will depress the location of the line.

Various cues acquired by a helicopter pilot from depth perception at low altitudes may be evaluated from Fig. 21. If we assume a static situation, i.e., imply a motionless hover, which is virtually never achieved, and peripheral stereopsis (θ_d = 70 seconds), stereoscopic cues are useful up to distances of about 30 feet (point A) beyond which retinal size differential $\Delta\epsilon/\epsilon$ takes over as the dominant cue. If central vision is involved, i.e., the pilot fixates to determine depth changes in or near his foveal field, so that the low threshold of θ_d = 10 seconds may be expected, this crossover point moves out to about 210 feet (point B).

If the helicopter has a lateral speed as low as 1 knot, and the pilot does not fixate for depth cues, motion parallax will be the dominant cue at distances up to about 160

feet (point C), from which point size will take over. For a longitudinal speed of 1 knot, and objects located about 10° below or to the side of the direction of motion, movement parallax will be the dominant cue until about 57 feet (point D), unless the pilot fixates on these objects. In the latter case, stereopsis will be dominant up to a distance of 220 feet (point B). The distances noted are estimates based on the use of standard deviations as thresholds. The statistical variations in Δr produced by randomly varying thresholds must be used to obtain the statistical properties of the perceptual processes in more detail.

Stereopsis Related to the Head-Up Display

The use of collimated images in a head-up display in a helicopter, from which the ground will be seen frequently at short distances, raises some interesting visual considerations. If there are no appreciable binocular disparities in the optical system of the head-up display, and the exit pupil permits the images to be viewed binocularly, the head-up display images will be seen emmetropically (with relaxed accommodation and no convergence of the eyes). If the imagery is superimposed on the terrain at close distances, the pilot will fixate on the ground and the head-up display images in the two eyes will be disparate. The stereoscopic effect is one in which the images are behind or below the ground, at visual infinity. This probably will not be the prevailing perceptual phenomenon, however, because there are other cues to the perception of distance in addition to stereopsis. These will localize the head-up display imagery near and in front of the ground plane. Nevertheless, considering stereopsis alone, the minimum comfortable distance for viewing the terrain and the head-up display images simultaneously may be determined. If a convergent binocular disparity tolerance of 2.5 mrad is assumed based on visual comfort, the minimum comfortable sustained viewing distance to the ground is that range at which the fixation angle (θ_f) is 2.5 mrad, or

$$r_f = \frac{p}{\theta_f} = \frac{0.213}{0.0025} = 85 \text{ feet},$$

where p is the interpupillary distance. This distance corresponds to an eye level height of 22 feet above the ground for a visual depression angle of 15° for the imagery in the head-up display. Any divergent disparity built into the optical system of the head-up display will lower the permissible fixation angle θ_f and raise the minimal distance d. These considerations cease to apply when the head-up images are viewed monocularly, due to either a smaller exit pupil or a shift in the pilot's head position.

On the basis of the foregoing, there is no indication that the use of collimated head-up display imagery superimposed on the terrain being viewed at short distances by a helicopter pilot will introduce visual discomfort, even when stereopsis is effective in depth discrimination at these ranges. This conclusion is also supported by the experience of the writer and his associates in looking at head-up displays in laboratory situations on the ground.

Regarding the perception of distance from the helicopter, the head-up display provides the pilot with a unique visual aid for estimating distances to targets of known size. The angular subtenses of most of the images in the display remain constant. Therefore, a particular image will be equal to the retinal size of a target only at one range or a given multiple of it. The visual task involved is a simple discrimination or comparison between a displayed image and an object in the real world viewed simultaneously. The pilot can readily learn to correlate this visual match with distance. As an example, consider a circular landing pad 70 feet in diameter. Assume a head-up display has an image such as a path

marker which has a width of 5 degrees. The path marker will fill the landing pad circle when the aircraft is about 800 feet from the center of the landing pad. It will be twice the size of the pad at 1600 feet, and half the size of the pad at 400 feet. This inverse size/distance relationship is accurate for the small angular subtenses involved.

FIELD OF VIEW REQUIREMENTS FOR HEAD-UP DISPLAYS IN HELICOPTERS

A procedure for determining the angular subtenses of the visual field to be covered by the images projected in a helicopter head-up display will be described in this section. For a particular aircraft, the required field of view depends on the flight regime of the vehicle, the flight maneuvers to be executed, and the external visual references necessary to conduct the operations. Under visual flight conditions (VFR), the pilot has fairly complete visual access to the environment around his aircraft, limited only by the attitude and heading of the vehicle and the visual cockpit cutoff angles. The field-of-view requirements for VFR are determined, therefore, by the relationships among the display images, the orientation of the aircraft, and the location of visual objects in the real world to be used in conjunction with the head-up display.

Consider, for example, a visual approach to a landing pad at a prescribed descent angle, using a deviation image to measure displacement from the reference path and a flight path marker to show the direction of flight (Fig. 22). The required field of view will be determined by the range of orientations of the deviation bar and flight path marker in the head-up display, and the landing aim point on the ground, for the attitudes and positions of the aircraft which may be involved in the approach maneuvers. In this case, the aim point must be contained within the field of the head-up display, because head-up display imagery is being used to overlay and/or overfly this point. In other VFR situation . such as clearing an obstacle, it may be sufficient to observe the visual target (obstacle) in the real world beyond the limits of the head-up display, and to execute maneuvers in relation to the target, which will ultimately move into the head-up display field. In VFR, therefore, not all key visual elements in the real world need be viewed through the head-up display to permit effective flight control and/or monitoring in relation to these elements. The head-up display augments the information derived from the visual world in VFR, and it need not present a complete display of the visual situation. In fact, such a complete display may introduce visual clutter and/or occlude visual targets in VFR operations.

Under instrument flight conditions (IFR), however, the surrogate images representing, for example, the landing area or a ground target with a known location must be presented in the head-up display in their correct visual position with respect to the aircraft. This is essential to make IFR flight compatible with VFR, so that the displays will be effective in mixed or limited visibility weather, for which the transitions between instrument and visual flight must be smooth. The field-of-view requirements under these conditions are generally larger than for visual flight alone.

There are several additional considerations involved in defining the visual field angles to be specified for the projection system of a head-up display. The installation of the head-up display in a cockpit is designed to minimize field requirements by optimizing the orientation of the center of the head-up display field. Thus, if the lower limit of the field is farther below the boresight line of the aircraft than the upper limit is above this reference, the center of the head-up display field should be depressed below the boresight line. In addition, the head-up display optics may be made movable, either in discrete steps to

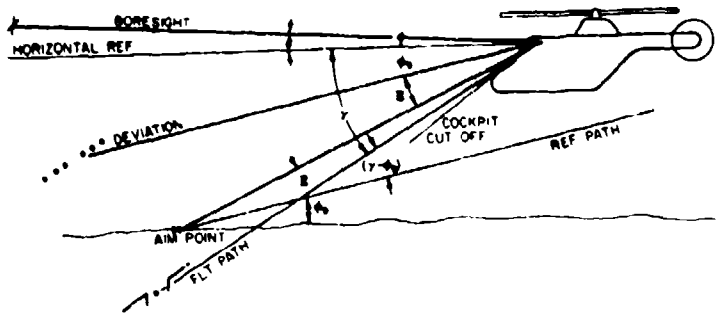

Fig. 22—Vertical viewing angles in visual landing approach

fixed positions or continuously adjustable, to cover different fields with respect to the aircraft for various flight modes. As an example, the head-up display may be in an "up" orientation for flight and "down" for approach and landing. Special flashing surrogate symbols may be oriented at the edges of the head-up display field to designate elements which are beyond the limits of the field. These may serve as adequate indicators for control until the targets move into the head-up display field. This technique is useful for operations in both VFR and IFR.

In most head-up display projector designs, the pilot's eyes are behind the exit pupil. This optical situation provides the pilot with dual overlapping monocular fields, displaced laterally by the separation between the eyes (interpupillary distance). The common field in the overlapping region is seen binocularly by the pilot. The field that is mapped by the image generator in a head-up display is generally larger than the instantaneous field seen by the pilot in one head position. The pilot can therefore extend the useful field of view in the head-up display with some head movement. Some of these visual considerations related to the design of head-up display systems are described in Ref. 17.

As an example of the required orientation of the head-up display images in the vertical plane, consider the approach for landing shown in Fig. 22. The desired approach angle to the aim point is ϕ_0, and the maximum angular deviation from the reference path is ϵ. If γ is the flight path angle of the aircraft, and this flight path is to intercept the reference path at an angle proportional to ϵ,

$$(\gamma - \phi_0) = a\epsilon, \tag{15}$$

where $(\gamma - \phi_0)$ is the intercept angle and a is a constant greater than unity. The flight path marker therefore has a maximum depression below the horizontal reference of

$$\gamma_1 = \phi_0 + a\epsilon, \tag{16}$$

which corresponds to a depression below the boresight line of

$$\theta_{\gamma 1} + \gamma_1 = \theta_{\gamma 1} + \phi_0 + a\epsilon, \tag{17}$$

where $\theta_{\gamma 1}$ is the pitch of the aircraft at a flight path angle of

$$\gamma_1 = \phi_0 + a\epsilon.$$

The preceding analysis covers the situation in which the aircraft intercepts the desired flight path from above. When the approach is initiated from below the reference path, the intercept angle is $(\phi_0 - \gamma)$, which is also made equal to $a\epsilon$. Under these conditions, the flight path marker has the minimum depression at an angle of

$$\gamma_2 = \phi_0 - a\epsilon, \tag{18}$$

which corresponds to a depression below the boresight of

$$\theta_{\gamma 2} + \gamma_2 = \theta_{\gamma 2} + \phi_0 - a\epsilon, \tag{19}$$

where $\theta_{\gamma 2}$ is the pitch of the aircraft at a flight path angle $\gamma_2 = (\phi_0 - a\epsilon)$. These required field limits for the path marker pertain to a single approach path ϕ_0. The deviation image is oriented at depression angles $(\theta_{\gamma 1} + \phi_0)$ and $(\theta_{\gamma 2} + \phi_0)$ for the same situations above and below the reference path. The required field of view for the head-up display and its orientation in the aircraft are determined by this type of analysis covering the full range of approach angles ϕ_0 which may be required with the head-up display. The envelope of these image orientations will determine the required field of view for the head-up display in the vertical plane.

As an example of the procedure for determining the field-of-view requirements in azimuth, consider the final-approach situation depicted in Fig. 23. The aircraft is approaching the landing pad by coupling to a reference path which will permit a landing into the wind at heading H. The initial lateral angular deviation of the aircraft from the reference path is δ and the desired intercept angle of the ground speed vector (path marker) is λ, which is assumed proportional to δ, i.e., $\lambda = b\delta$. The relationship among air speed, ground speed, and wind is shown by the vector diagram in Fig. 23. The associated sideslip angle of the helicopter at the approach speed is shown as β. The half-field angle required for the head-up display under these conditions is either ψ or $(\lambda - \psi)$, whichever is greater. The angle λ is determined by the maximum deviation angle δ, from which ψ can be determined from the velocity vector relationships. The required field of view will be based on the envelope of the image positions.

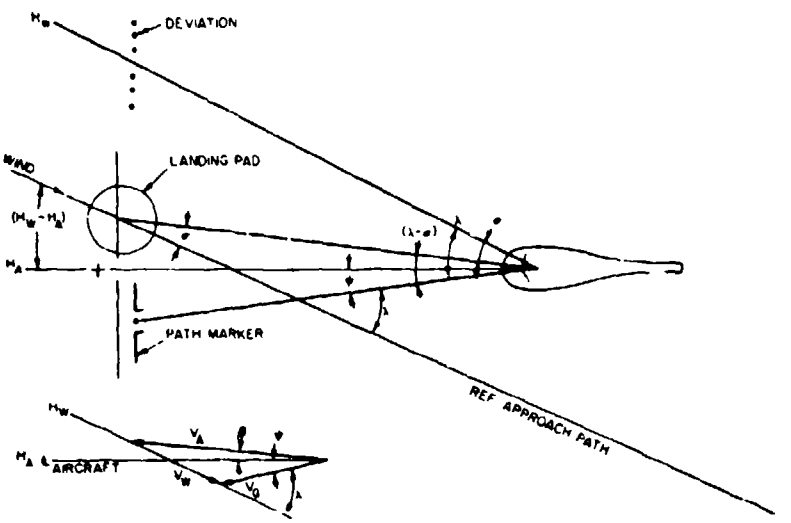

Fig. 23—Horizontal viewing angles in visual landing approach

The application of these procedures to flight operations with particular helicopter types requires pitch, roll, and sideslip data at various climb angles, level flight, and descent angles over a range of gross weights and the speed regime of the aircraft. Unfortunately, there is a very limited data of this type currently available from the airframe manufacturers. Emphasis in flight testing to date is on aerodynamic and structural measurements, with minimal data obtained relating aircraft orientation with respect to earth axes. Also, some of these data are sensitive to pilot control techniques, e.g., the tradeoff between sideslip and roll angle, since helicopter flight is always more or less unsymmetrical. On this basis, the optimal selection of head-up display fields must await the availability of more helicopter flight test and/or analytical data of the type noted. However, there has been an approximation made to the total field requirements for an H-53 helicopter in VFR/IFR operations, based on a few estimates for orientation angles made by the airframe manufacturer (17). The flight maneuvers considered climb/cruise, terrain following, and approach/hover, and the results are shown in Fig. 24. These are comprehensive requirements for an advanced display, with sophisticated sensors and data processors. The field angles would be appreciably lower for a simpler head-up display to be used principally in visual flight.

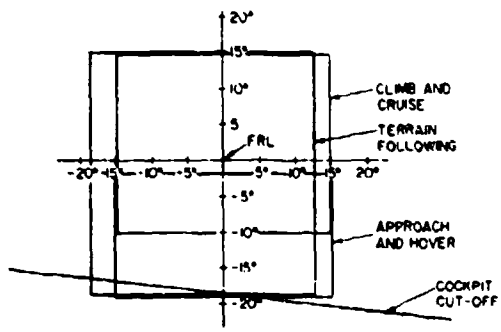

Fig. 24—Field of view requirements for VFR/IFR head-up display for H-53 aircraft

CONCLUSIONS

1. The maximum permissible binocular disparities for moving head-up display images, viewed with adequate visual comfort against a dynamic, real world background, are 1.0 milliradian for vertical disparities and convergent horizontal disparities and 2.5 milliradians for divergent horizontal disparities.

2. The presence of a dynamic real world background does not affect binocular disparity tolerances, which are the same when head-up display images are viewed against a static real world background.

3. The results of Maddox Rod tests for phorias and ductions performed in optometric examinations correlate well with pilots' tolerances to binocular disparities in head-up displays.

4. The limiting distances for the use of stereopsis in depth perception in the real world have been determined for helicopter pilots on both static and dynamic platforms. Differential size and motion parallax are the principal monocular cues to depth which dominate in simple visual situations when the stereopsis cues become weak.

5. The use of collimated images in head-up displays will not produce visual difficulties for the helicopter pilot when he simultaneously views the ground at the short distances for which stereopsis is an effective cue for depth perception.

6. A procedure for determining the field of view required in a head-up display for a helicopter with its mission envelope has been developed.

REFERENCES

1. T. Gold and A. Hyman, "Visual Requirements Study for Head-Up Displays," Sperry Rand Corporation, Sperry Gyroscope Division, Final Report for Phase I, SGD-4283-0333, JANAIR Report 680712, Office of Naval Research, Washington, D.C., Mar. 1970.

2. J.J. McGrath and G.J. Borden, "Geographic Orientation in Aircraft Pilots: A Research Method," Technical Report 751-2, Human Factors Research, Inc., Santa Barbara, California, Sept. 1964.

3. J.J. McGrath et al., "Geographic Orientation in Aircraft Pilots: Methodological Advancement," Technical Report 751-5, Human Factors Research, Inc., Santa Barbara, California, Oct. 1965.

4. M. Schapero, D. Cline, and H.W. Hofstetter, editors, *Dictionary of Visual Science*, Philadelphia, Chilton, 1968.

5. S. Siegel, *Nonparametric Statistics for the Behavioral Sciences*, New York, McGraw Hill, 1956.

6. K.N. Ogle, *Research in Binocular Vision*, Philadelphia, Saunders, 1950; reprinted by Hafner, New York, 1964.

   This extensive work in binocular vision has a comprehensive bibliography with 259 sources cited. The reprinted edition has an additional list of 67 pertinent references which have appeared between 1950 and 1963.

7. C.H. Graham, editor, *Vision and Visual Perception*, New York, Wiley, 1965.

8. K.N. Ogle, "Theory of Stereoscopic Vision," in *Psychology: Study of a Science, Volume 1, Sensory Perceptual and Physiological Formulation*, S. Koch, editor, New York, McGraw Hill, 1959.

9. J.J. Gibson, *The Perception of the Visual World*, Boston, Houghton Mifflin, 1950.

10. K.N. Ogle, "Precision and Validity of Stereoscopic Depth Perception from Double Images," J. Opt. Soc. Am. 43, 906 (1953).

11. K.N. Ogle, "On the Limits of Stereoscopic Vision," J. Exper. Psychol. 44, 253 (1957).

12. K.N. Ogle, "Some Aspects of Stereoscopic Depth Perception," J. Opt. Soc. Am. 57, 1073 (1967).

13. J.P. Guilford, *Psychometric Methods*, 2nd edition, New York, McGraw Hill, 1954.

14. W.H. Teichner, J.L. Kobrick, and R.F. Wehrkamp, "The Effects of Terrain and Observation Distance of Relative Depth Discrimination," Am. J. Psychol. 68, 193-208 (1955).

15. M.J. Hirsch and F.W. Weymouth "Distance Discrimination: V. Effect of Motion and Distance of Targets on Monocular and Binocular Distance Discrimination," J. Aviat. Med. 18, 594-600 (1947).

16. T. Gold, "A Psychophysical Study of the Gestalt Proximity Law of Perceptual Organization," presented at the Annual Meeting of the Eastern Psychological Association, Philadelphia, Pennsylvania, Apr. 1961.

17. Anon. "Head-Up Display Study for Helicopter/STOL Aircraft," Sperry Flight Systems Division, Phoenix, Arizona (to be published).

APPENDIX A

GEOMETRY FOR STEREOPSIS

The geometrical relationships involved in stereoscopic vision may most easily be appreciated by considering the simple situation in Fig. A1. Points 1 and 2 are being observed binocularly by the left and right eyes, L and R. Point 2 is located behind point 1 on a line from the center of rotation of the right eye (O_R), at right angles to the line between the centers of rotation of both eyes ($O_L O_R$). Therefore, points 1 and 2 are imaged on the same point (fovea) on the retina of the right eye. If it is assumed that the distances from which points 1 and 2 are viewed are large in relation to the interpupillary distance p, the angles in Fig. A1 will all be small, so that the approximation $\tan \theta \approx \sin \theta \approx \theta$ is valid, and the trigonometric relations can be simplified. The angles are expressed in radians in these equalities.

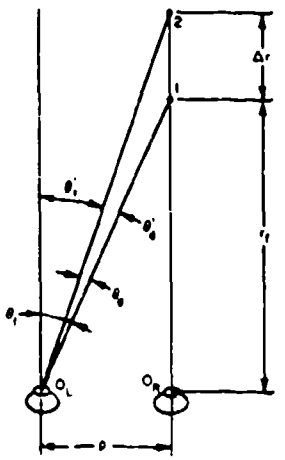

Fig. A1—Basic geometry for stereopsis

If the eyes are fixated at point 1, the convergence angle θ_f is given by

$$\theta_f = p/r_f. \tag{A1}$$

In Fig. A1, we have a case of asymmetric convergence since point 1 is not symmetrically oriented with respect to both eyes. The binocular disparity θ_d, associated with the difference in depth Δr between points 1 and 2, may be determined by

$$\theta_f - \theta_d = p/(r_f + \Delta r) \tag{A2a}$$

or
$$\theta_d = \theta_f - p/(r_f + \Delta r) = p/r_f - p/(r_f + \Delta r)$$
$$= \left(\frac{p}{r_f}\right)\left(\frac{\Delta r}{r_f + \Delta r}\right). \quad \text{(A2b)}$$

This may be expressed as

$$\theta_d = \theta_f \delta_r, \quad \text{(A3)}$$

where δ_r is the depth ratio $[\Delta r/(r_f + \Delta r)]$.

If the observer were to fixate at point 2, the fixation angle would be

$$\theta'_f = p/(r_f + \Delta r) \quad \text{(A4)}$$

and

$$\theta'_d + \theta'_f = p/r_f \quad \text{(A5)}$$

so that

$$\theta'_d = p/r_f - \theta'_f = p/r_f - p/(r_f + \Delta r)$$
$$= \left(\frac{p}{r_f}\right)\left(\frac{\Delta r}{r_f + \Delta r}\right). \quad \text{(A6)}$$

Since θ'_d from Eq. (A6) is identical to θ_d in Eq. (A2b), the magnitude of the disparity is independent of the fixation point.

Equation (A2b) for the binocular disparity θ_d has been developed for the situation in Fig. A1, in which points 1 and 2 are aligned with one eye. A more general situation is shown in Fig. A2. The angular separations between points 1 and 2 as seen by the left and right eyes are the parallax angles α_L and α_R. For the small angles involved,

$$\alpha_L = \frac{p + \omega}{r_f} - \frac{p + \omega}{r_f + \Delta r} = \frac{(p + \omega)\Delta r}{r_f(r_f + \Delta r)} \quad \text{(A7)}$$

and

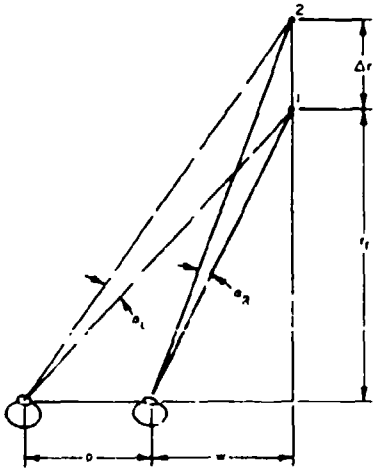

Fig. A2—Generalized situation for stereopsis

$$\alpha_R = \frac{\omega}{r_f} - \frac{\omega}{r_f + \Delta r} = \frac{\omega \Delta r}{r_f(r_f + \Delta r)}. \tag{A8}$$

The binocular disparity is the difference between the parallax angles α_L and α_R, so that

$$\theta_d = \alpha_L - \alpha_R = \left(\frac{p}{r_f}\right)\left(\frac{\Delta r}{r_f + \Delta r}\right), \tag{A9}$$

which agrees with Eq. (A2b).

Note from Fig. A2 that, when points 1 and 2 are the same distance from the eyes but separated laterally, the parallax angles α_L and α_R are equal. The binocular disparity will then be zero. The binocular disparity is therefore seen to be generated by differences in depth Δr; it is unaffected by lateral position for the small angles which are being considered.

When a point (Fig. A3) is at a very large distance beyond point 1 (visual infinity), Eq. (A2b) indicates that

$$\lim_{\Delta r \to \infty} \theta_d = \lim_{\Delta r \to \infty} \left(\frac{p}{r_f}\right)\left(\frac{\Delta r}{r_f + \Delta r}\right) = \frac{p}{r_f} = \theta_f. \tag{A10}$$

Therefore, the binocular disparity approaches the convergence angle θ_f under these conditions. The same numerical result is obtained for the disparity when the eyes are fixated at visual infinity (Fig. A4) so that

$$\theta_d = \alpha_L - \alpha_R = \frac{p + \omega}{r} - \frac{\omega}{r} = \frac{p}{r}, \tag{A11}$$

where r is the distance of the disparate point from the eyes.

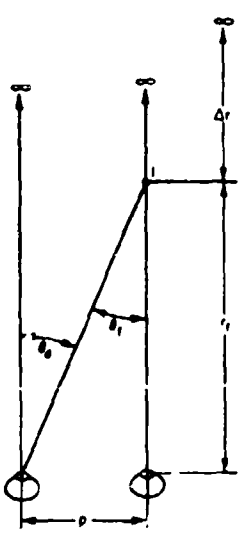

Fig. A3—Stereopsis with far point at visual infinity

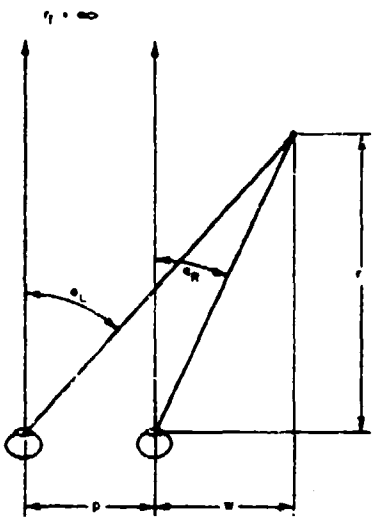

Fig. A4—Stereopsis with fixation point at visual infinity

Equation (A3) indicates that the disparity is equal to the fixation angle multiplied by the depth ratio δ_r; i.e.,

$$\theta_d = \theta_f \delta_r = \theta_f \left(\frac{\Delta r}{r_f + \Delta r} \right). \tag{A12}$$

The depth ratio is always less than one and approaches unity as Δr becomes very large in relation to r_f. The maximum disparity possible is the fixation angle θ_f. If the ratio $(\Delta r / r_f)$, the relative incremental depth, is designated as β, then the depth ratio is related to β, from Eq. (A12) by

$$\delta_r = \beta/(1 + \beta). \tag{A13}$$

It is convenient to represent the preceding relationships graphically. These are shown in Figs. A5 through A7, on three-cycle log paper to cover ranges of values with a ratio of 1000:1. Disparity θ_d in seconds of arc is plotted as a function of fixation range r_f in feet with δ_r as a parameter (Eq. (A12)) in Fig. A5. Associated values of Δr in feet are also presented in Fig. A5 by the dashed series of lines. For a given set of values of r_f and Δr, θ_d may be determined more directly from the plot in Fig. A6. The curves in Fig. A6 for fixed values of θ_d are asymptotic to specific values of r_f and for large values of Δr. These values of r_f are equal to (p/θ_d), from Eq. (A2b), for values of $\Delta r >> r_f$. The asymptotic values of r_f are shown plotted as a function of θ_d as the dashed line in Fig. A6. Finally, the depth ratio δ_r is shown plotted as a function of β in Fig. A7. This curve shows δ_r approaching unity for large values of β. The interpupillary distance p has been taken as 65 mm, or 0.213 feet, in the computations for the plots.

The factor $[\Delta r / r_f (r_f + \Delta r)]$ occurs frequently in relationships for stereopsis and monocular motion parallax (Appendix B). This factor, which has the dimension 1/ft, will be designated by the term depth factor, and given the symbol K_r. The depth factor is plotted as a function of r_f and Δr in Fig. A8.

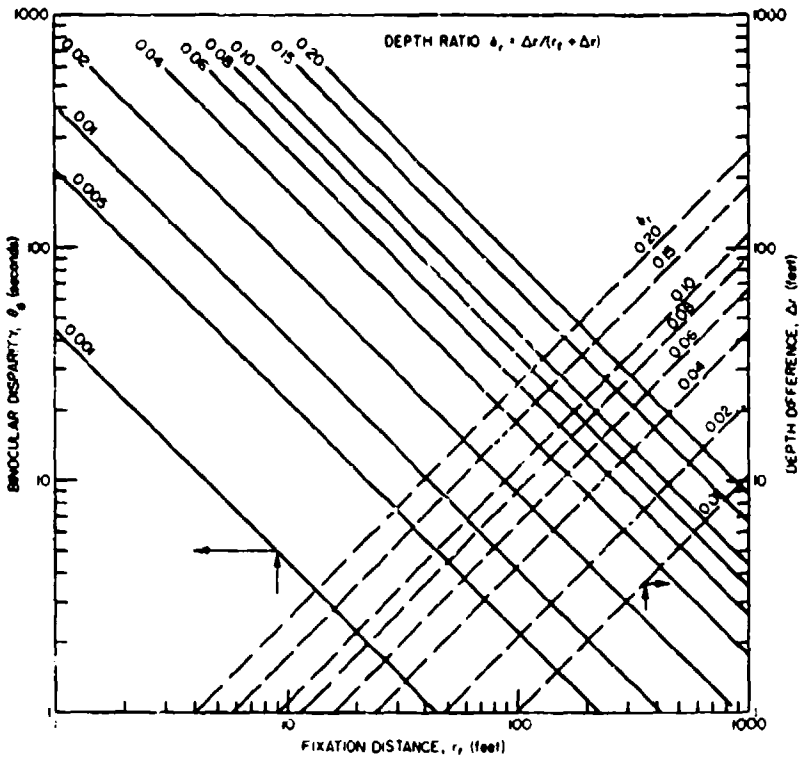

Fig. A5—Binocular disparities as a function of distance, depth difference, and depth ratio

The binocular disparity in Eq. (A2b) is often expressed by the approximation

$$\theta_d'' = p\Delta r/r_f^2. \tag{A14}$$

This is an overestimation by an amount

$$\begin{aligned}\Delta\theta_d = \theta_d'' - \theta_d &= p\Delta r\left[\frac{1}{r_f^2} - \frac{1}{r_f(r_f+\Delta r)}\right] \\ &= p\Delta r\left[\frac{\Delta r}{r_f^2(r_f+\Delta r)}\right]\end{aligned} \tag{A15}$$

so that the relative error $(\Delta\theta_d/\theta_d)$ reduces to $(\Delta r/r_f)$. Therefore, the approximation for the binocular disparity in Eq. (A14) produces a relative error equal to the relative incremental depth β (Eq. (A13)).

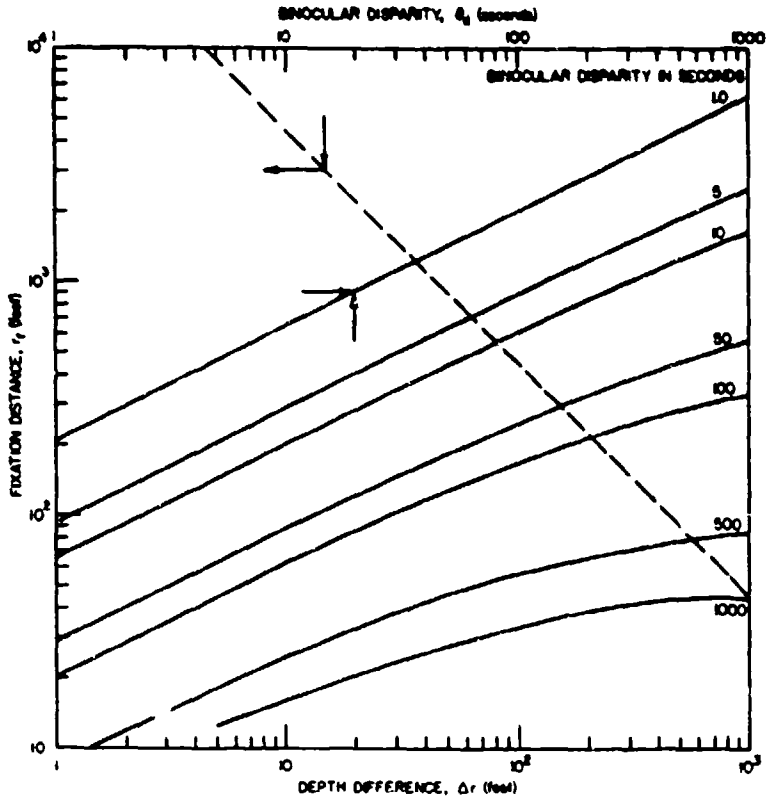

Fig. A6—Depth differences and distances associated with several binocular disparities

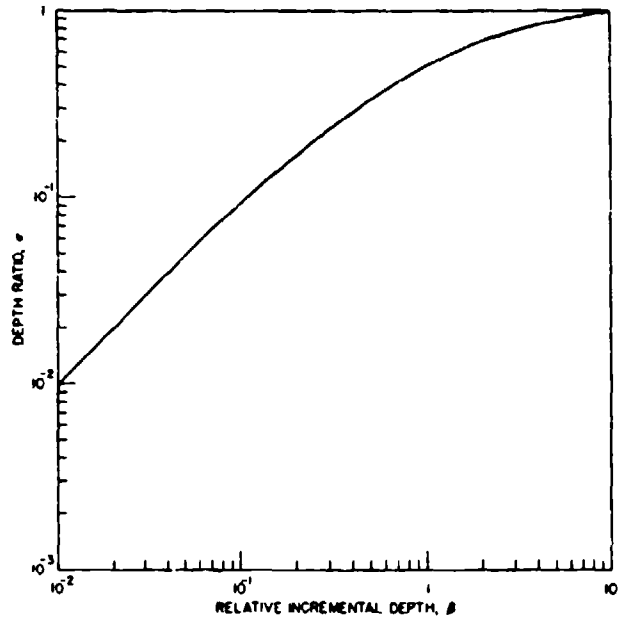

Fig. A7—Depth ratio as a function of relative incremental depth

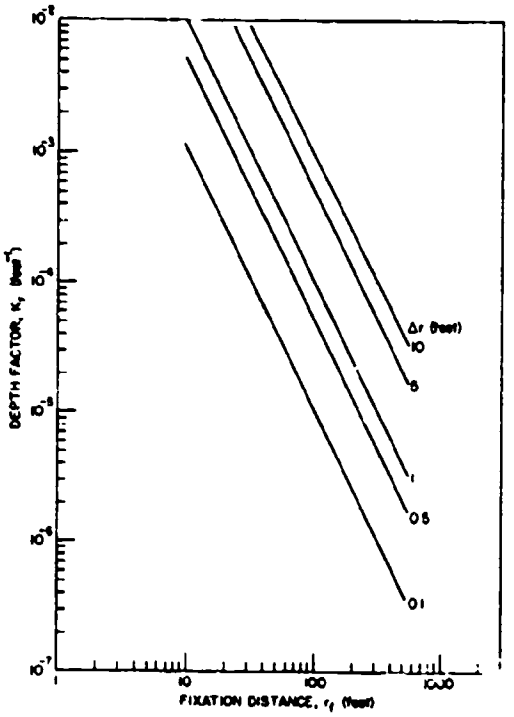

Fig. A8—Depth factor K_r as a function of distance and depth difference

APPENDIX B

MOTION PARALLAX

Movement parallax is the differential angular velocity between the lines of sight from an observer to two objects, one of which is fixated by the observer. This situation is shown statically in Fig. B1, where the lines of sight from one eye to points 1 and 2 are θ_1 and θ_2.

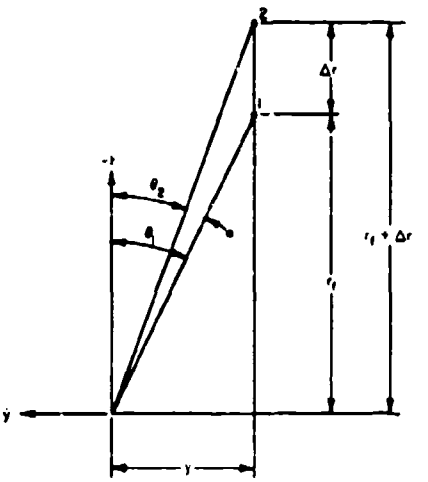

Fig. B1—Basic geometry for motion parallax

It has already been demonstrated (page 33) that a binocular disparity may be considered as a difference between the parallax angles of two objects to the two eyes of the observer. This relationship between binocular disparity and parallax will be investigated further in the following analysis. If we refer to Fig. B1, where monocular parallax is depicted, for small angles θ,

$$\theta_1 = y/r_f \text{ and } \theta_2 = y/(r_f + \Delta r). \tag{B1}$$

The parallax angle α is therefore given by

$$\alpha = \theta_1 - \theta_2 = y\left[\frac{1}{r_f} - \frac{1}{(r_f + \Delta r)}\right] = y\left[\frac{\Delta r}{r_f(r_f + \Delta r)}\right]. \tag{B2}$$

First, consider lateral motion $\dot{y} \equiv dy/dt$. From Eq. (B2) since the distances r remain constant for lateral motion,

$$\dot{\alpha}_y = \dot{y}\left[\frac{\Delta r}{r_f(r_f + \Delta r)}\right] = \frac{\alpha}{y}\dot{y} \tag{B3a}$$

or

$$\dot{\alpha}_y/\alpha = \dot{y}/y. \tag{B3b}$$

Therefore, for lateral motion, which is defined as normal to the line joining two points in planar visual space, the relative rate of change of the monocular parallax angle ($\dot{\alpha}_y/\alpha$) is equal to the relative rate of change of lateral displacement from the two points ($\dot{y}/y$).

For the binocular situation (Fig. A2) the movement parallax for the left eye, based on the lateral motion $\dot{y}$, is

$$\dot{\alpha}_{Ly} = \alpha_L \frac{\dot{y}}{y+p}. \tag{B4}$$

Similarly, for the right eye,

$$\dot{\alpha}_{Ry} = \alpha_R \dot{y}/y. \tag{B5}$$

By substituting values of α_L and α_R determined from Eq. (B2) in Eqs. (B4) and (B5)

$$\dot{\alpha}_{Ly} = \dot{y}\left(\frac{\Delta r}{r_f + \Delta r}\right) \text{ and } \dot{\alpha}_{Ry} = \dot{y}\left(\frac{\Delta r}{r_f + \Delta r}\right). \tag{B6}$$

Therefore, since $\dot{\alpha}_{Ly} = \dot{\alpha}_{Ry}$ the movement parallax for lateral motion is the same for both eyes. The rate of change of binocular disparity is zero since

$$\dot{\theta}_d = \dot{\alpha}_{Ly} - \dot{\alpha}_{Ry} = 0. \tag{B7}$$

The monocular movement parallax for longitudinal motion may also be determined from Fig. B1. From Eq. (B2)

$$\alpha = y\left[\frac{1}{r_f} - \left(\frac{1}{r_f + \Delta r}\right)\right]. \tag{B8}$$

Differentiating Eq. (B8) with respect to time, recognizing that $\dot{y} = 0$ and

$$\dot{r}_f = \overline{(r_f + \Delta r)} = \dot{r},$$

$$\dot{\alpha}_r = y\dot{r}\left[-\frac{1}{r_f^2} + \frac{1}{(r_f + \Delta r)^2}\right] = -\alpha\dot{r}\left[\frac{1}{r_f} + \frac{1}{(r_f + \Delta r)}\right]. \tag{B9}$$

Therefore,

$$\dot{\alpha}_r/\alpha = -\dot{r}\left[\frac{1}{r_f} + \frac{1}{(r_f + \Delta r)}\right] = -2\frac{\dot{r}}{r_h}, \tag{B10}$$

where r_h is the harmonic mean distance to the two points, i.e.,

$$1/r_h = 1/2\,[1/r_f + 1/(r_f + \Delta r)].$$

For longitudinal motion, the relative rate of change of monocular parallax angle ($\dot{\alpha}_r/\alpha$) is numerically equal to twice the relative rate of longitudinal displacement taken with respect to the harmonic mean distance (r_h).

If we consider binocular effects, the motion parallaxes for the left and right eyes are, from Eq. (B10)

$$\dot{\alpha}_{Lr} = \alpha_L \left(-2\frac{\dot{r}}{r_h}\right) \text{ and } \dot{\alpha}_{Rr} = \alpha_R \left(-2\frac{\dot{r}}{r_h}\right). \tag{B11}$$

The rate of change of binocular disparity $\dot{\theta}_{d_r}$ is therefore

$$\dot{\theta}_{dr} = \dot{\alpha}_{Lr} - \dot{\alpha}_{Rr} = -2\frac{\dot{r}}{r_h}(\alpha_L - \alpha_R) = -2\frac{\dot{r}}{r_h}\theta_d \tag{B12}$$

since $\alpha_L - \alpha_R = \theta_d$. Consequently

$$\dot{\theta}_{dr}/\theta_d = -2\frac{\dot{r}}{r_h}. \tag{B13}$$

Equation (B13) indicates that the relative binocular disparity rate ($\dot{\theta}_{dr}/\theta_d$) is twice the relative range rate ($\dot{r}/r_h$) and is therefore equal to the relative rate of change of monocular motion parallax ($\dot{\alpha}_r/\alpha$) for longitudinal motion of the observer (Eq. (B10)).

In general, the motion of an observer with respect to two points in space has both lateral and longitudinal components (Fig. B2). Under these conditions, the monocular motion parallax $\dot{\alpha}$ must be determined by considering the total derivative of α with respect to time

$$\frac{dx}{dt} = \frac{\partial\alpha}{\partial y}\cdot\frac{dy}{dt} + \frac{\partial\alpha}{\partial r}\cdot\frac{dr}{dt}$$

or (B14)

$$\dot{\alpha} = \frac{\partial\alpha}{\partial y}\cdot\dot{y} + \frac{\partial\alpha}{\partial r}\cdot\dot{r}.$$

However, the two terms on the right-hand side of Eq. (B14) are the values of $\dot{\alpha}_y$ (Eq. (B3)) and $\dot{\alpha}_r$ (Eq. (B9)). Therefore,

$$\dot{\alpha} = \dot{\alpha}_y + \dot{\alpha}_r = \left[-\frac{\Delta r}{r_f(r_f + \Delta r)}\right]\dot{y} + \left[\frac{y\Delta r}{r_f(r_f + \Delta r}\right]\left(-\frac{2}{r_h}\right)\dot{r}$$

$$= K_r\dot{y} + K_r y\left(-\frac{2}{r_h}\right)\dot{r}, \tag{B15}$$

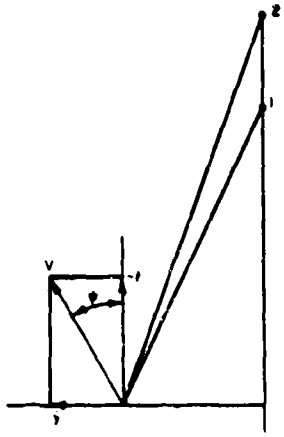

Fig. B2—Generalized motion parallax

where the depth term $\Delta r/r_f(r_f + \Delta r)$ is designated by K_r. From Fig. B2, the lateral and longitudinal rates are

$$\dot{y} = V \sin \psi \text{ and } \dot{r} = -V \cos \psi.$$

Therefore, substituting these values into Eq. (B15) yields

$$\begin{aligned} \dot{\alpha} &= K_r V \sin \psi + K_r y \left(-\frac{2}{r_h}\right)(-V \cos \psi) \\ &= VK_r \left(\sin \psi + \frac{2y}{r_h} \cos \psi\right). \end{aligned} \tag{B16}$$